

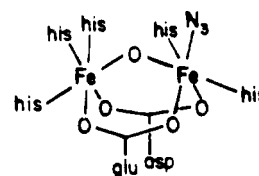
# Assembly and Characterization of an Accurate Model for the Diiron Center in Hemerythrin

William H. Armstrong,<sup>1a</sup> Alan Spool,<sup>1a</sup> Georgia C. Papaefthymiou,<sup>1b</sup>  
Richard B. Frankel,<sup>1b</sup> and Stephen J. Lippard\*<sup>1a</sup>

Contribution from the Department of Chemistry and the Francis Bitter National Magnet Laboratory, Massachusetts Institute of Technology, Cambridge, Massachusetts 02139.  
Received December 28, 1983

**Abstract:** Using either simple ferric salts or the preassembled ( $\mu$ -oxo)diiron(III) anion,  $[\text{Cl}_3\text{FeOFeCl}_3]^{2-}$ , bridged binuclear complexes  $[(\text{HBpz}_3)\text{FeO}(\text{O}_2\text{CR})_2\text{Fe}(\text{HBpz}_3)]$ ,  $\text{R} = \text{H}, \text{CH}_3, \text{C}_6\text{H}_5$  and  $\text{HBpz}_3 = \text{tri-1-pyrazolylborate}$  ion, were prepared. X-ray crystallographic studies of the acetate and formate derivatives revealed a structure in which the two iron atoms are linked by a  $\mu$ -oxo and two  $\mu$ -carboxylato bridging ligands in a bioctahedral geometry in which the termini are capped by the tridentate tri-1-pyrazolylborate ligands. The geometry of the  $\{\text{Fe}_2\text{O}(\text{O}_2\text{CR})_2\}$  core of these compounds is nearly congruent with that found in the azidomet forms of the marine invertebrate oxygen transport proteins, hemerythrin and myohemerythrin. The ( $\mu$ -oxo)diiron(III) center is bent, with an average Fe-O bond length of 1.783 (3) Å and an average Fe-O-Fe angle of 124.6 (1)°. The vibrational modes of this center have been characterized by extensive Raman, resonance Raman, and Fourier transform infrared (FTIR) spectroscopic studies of the model complexes and their <sup>18</sup>O analogues. The latter were prepared by exchange with <sup>18</sup>OH<sub>2</sub>, which is a facile reaction. The asymmetric stretch ( $\nu_{\text{as}}$ ) occurs at 751 cm<sup>-1</sup> and is relatively weak. It underlies a strong HBpz<sub>3</sub><sup>-</sup> ligand band and shifts under another such band (to 721 cm<sup>-1</sup>) in the <sup>18</sup>O derivative. This behavior was mapped by difference FTIR spectroscopy. The symmetric stretch and deformation modes occur at 528 and 278 cm<sup>-1</sup>, respectively. These vibrational features as well as the magnetic exchange properties, ligand field bands in the optical spectrum (695 nm,  $\epsilon$  70 M<sub>Fe</sub><sup>-1</sup> cm<sup>-1</sup>; ~990 nm,  $\epsilon$  3.5 M<sub>Fe</sub><sup>-1</sup> cm<sup>-1</sup>), and Mössbauer spectroscopic parameters ( $\delta = 0.52 \pm 0.03$  mm/s;  $\Delta E_{\text{Q}} = 1.55 \pm 0.05$  mm/s) are compared to those reported for met- and oxyhemerythrin as well as other proteins believed to contain ( $\mu$ -oxo)diiron(III) cores. Proton NMR investigations of  $[\text{Fe}_2\text{O}(\text{O}_2\text{CCH}_3)_2(\text{HBpz}_3)_2]$  and its deuterated analogues are reported in which the paramagnetically shifted acetate group methyl proton resonances are identified at -10.5 ppm. This assignment should facilitate location of the analogous resonance in the proteins. Cyclic voltammetric studies of  $[\text{Fe}_2\text{O}(\text{O}_2\text{CCH}_3)_2(\text{HBpz}_3)_2]$  revealed an irreversible reduction accompanied by formation of mononuclear  $[\text{Fe}(\text{HBpz}_3)_2]$ , which itself undergoes a reversible one-electron oxidation. The instability of the ( $\mu$ -oxo)diiron(II) unit in the model compound parallels that of the reduced (deoxy) form of the protein. Magnetic susceptibility measurements on a SQUID susceptometer over the range  $2.9 < T < 300$  K revealed the diiron(III) center of  $[\text{Fe}_2\text{O}(\text{O}_2\text{CCH}_3)_2(\text{HBpz}_3)_2]$  to be antiferromagnetically coupled with a spin exchange coupling constant  $J = -121$  cm<sup>-1</sup>, a value close to that (-134 cm<sup>-1</sup>) of methemerythrin.

Oxo-bridged binuclear iron centers are ubiquitous in biology. They occur in the invertebrate oxygen transport proteins myohemerythrin<sup>2,3</sup> and hemerythrin,<sup>2,4</sup> in ribonucleotide reductase of *Escherichia coli*,<sup>5</sup> and in purple acid phosphatases from beef spleen<sup>6</sup> and pig allantoic fluid.<sup>7</sup> Structural details of the diiron sites of the metazido forms of hemerythrin from *Themiste dyscritum*<sup>4</sup> and myohemerythrin from *Themiste zostericola*<sup>3</sup> have been elucidated by X-ray crystallographic studies. Both have similar structures schematized in the drawing shown below. Two iron atoms are bridged by an oxo atom and by two carboxylate groups from the polypeptide chain. The remaining coordination



asp = aspartate; glu = glutamate; his = histidine

sites are occupied by three histidine imidazole groups for one iron atom and by two histidines and the azide ion for the other iron atom.

Although a large number of oxo-bridged binuclear iron complexes have been prepared and characterized,<sup>8</sup> most have only a single  $\mu$ -oxo bridge between iron atoms and therefore cannot be considered as realistic models for the hemerythrin diiron site. One proposed model compound for the hemerythrin core,  $(\text{C}_3\text{H}_{12}\text{N}_3)[(\text{CH}_3\text{COO})\{\text{Fe}(\text{C}_6\text{H}_4\text{O}_2)_2\}_2]$ ,<sup>9</sup> is a binuclear, monoacetato-bridged complex, which has no oxo bridge but contains bridging alkoxy groups from catecholate ligands. A potentially relevant  $\mu$ -oxo  $\mu$ -sulfato structure has been proposed for  $[\text{Fe}_2\text{O}(\text{phen})_2(\text{SO}_4)]\text{SO}_4 \cdot 6\text{H}_2\text{O}$  on the basis of infrared spectral data,<sup>10</sup> but it has not been proven by X-ray crystallography. Other binuclear iron complexes which may be of some structural relevance to hemerythrin include the ferric acetate species of Vasisht

(1) (a) Department of Chemistry. (b) Francis Bitter National Magnet Laboratory.

(2) (a) Klotz, I. M.; Klippenstein, G. L.; Hendrickson, W. A. *Science* **1976**, *192*, 335-344. (b) Kurtz, D. M., Jr.; Shriver, D.; Klotz, I. M. *Coord. Chem. Rev.* **1977**, *24*, 145-178. (c) Stenkamp, R. E.; Jensen, L. H. *Adv. Inorg. Biochem.* **1979**, *1*, 219-233. (d) Sanders-Loehr, J.; Loehr, T. M. *Ibid.* **1979**, *1*, 235-252. (e) Wilkins, R. G.; Harrington, P. C. *Ibid.* **1983**, *5*, 51-85. (f) Klotz, I. M.; Kurtz, D. M., Jr. *Acc. Chem. Res.* **1984**, *17*, 16-22.

(3) (a) Hendrickson, W. A. In "Invertebrate Oxygen-Binding Proteins: Structure, Active Site, and Function"; Lamy, J., Lamy, J., Eds.; Marcel-Dekker: New York, 1981; pp 503-515. (b) Hendrickson, W. A.; Sheriff, S.; Smith, J. L., private communication.

(4) (a) Stenkamp, R. E.; Sieker, L. C.; Jensen, L. H.; Sanders-Loehr, J. *Nature (London)* **1981**, *291*, 263-264. (b) Stenkamp, R. E.; Sieker, L. C.; Jensen, L. H. *J. Am. Chem. Soc.* **1984**, *106*, 618-622.

(5) (a) Thelander, L.; Reichard, P. *Annu. Rev. Biochem.* **1979**, *48*, 133-158. (b) Petersson, L.; Gräslund, A.; Ehrenberg, A.; Sjöberg, B.-M.; Reichard, P. *J. Biol. Chem.* **1980**, *255*, 6706-6712. (c) Sjöberg, B.-M.; Loehr, T. M.; Sanders-Loehr, J. *Biochemistry* **1982**, *21*, 96-102. (d) Reichard, P.; Ehrenberg, A. *Science* **1983**, *221*, 514-519. (e) Sjöberg, B.-M.; Gräslund, A. *Adv. Inorg. Biochem.* **1983**, *5*, 87-110.

(6) Davis, J. C.; Averill, B. A. *Proc. Natl. Acad. Sci. U.S.A.* **1982**, *79*, 4623-4627.

(7) (a) Antanaitis, B. C.; Aisen, P.; Lillenthal, H. R. *J. Biol. Chem.* **1983**, *258*, 3166-3172. (b) Sinn, E.; O'Connor, C. J.; de Jersey, J.; Zerner, B. *Inorg. Chim. Acta* **1983**, *78*, L13-L15.

(8) Reviews: (a) Gray, H. B.; Schugar, H. J. In "Inorganic Biochemistry"; Eichhorn, G., Ed.; Elsevier: New York, 1973; Chapter 3. (b) Murray, K. S. *Coord. Chem. Rev.* **1974**, *12*, 1-35.

(9) Anderson, B. F.; Webb, J.; Buckingham, D. A.; Robertson, G. B. *J. Inorg. Biochem.* **1982**, *16*, 21-32.

(10) (a) Jezowska-Trzebiatowska, B.; Ozarowski, A.; Kozłowski, H.; Cukierda, T.; Hanuza, J. *J. Inorg. Nucl. Chem.* **1976**, *38*, 1447-1450. (b) Jezowska-Trzebiatowska, B.; Hanuza, J.; Ozarowski, A.; Kozłowski, H. *Bull. Acad. Pol. Sci.* **1975**, *23*, 609-622.

and co-workers.<sup>11</sup> Oxo-bridged structures for these complexes can be ruled out on the basis of magnetic susceptibility measurements.

Prior to the work described here, there had been no report of an attempt to synthesize the ( $\mu$ -oxo)bis( $\mu$ -carboxylato)diiron(III) core as a model for the hemerythrin diiron site. Our approach resembles in some respects the "self-assembly" method<sup>12</sup> used by Holm and co-workers for the synthesis of dimeric,<sup>12</sup> trimeric,<sup>13</sup> tetrameric, and hexameric<sup>13</sup> iron-sulfur clusters. The bioctahedral structure of the diiron site in hemerythrin dictated the use of a facially coordinating tridentate amine ligand. We chose to work initially with tri-1-pyrazolylborate, owing to its ease of synthesis. This and a related ligand were employed to occupy three copper coordination sites in an earlier attempt to model the blue copper protein site.<sup>14</sup> In this paper we report the synthesis, structure, and physical properties of complexes formed either from simple ferric salts or from the "preformed"  $[\text{Fe}_2\text{OCl}_6]^{2-}$  ion in aqueous or acetonitrile mixtures containing potassium tri-1-pyrazolylborate and sodium carboxylate salts. Preliminary results for  $[\text{Fe}_2\text{O}(\text{O}_2\text{CCH}_3)_2(\text{HBpz}_3)_2]$  (**1**) were reported previously.<sup>15</sup> Presented for the first time here are the preparation of the formate (**2**) and benzoate (**3**) analogues, full details of the crystal structure determinations of **1** and **2**, and measurements of Mössbauer, Raman, infrared, electrochemical, and magnetic properties along with a comparison to the natural systems. EXAFS results will be discussed separately.<sup>16</sup> A second product from the aforementioned aqueous reaction mixture is the mononuclear cation,  $[\text{Fe}(\text{HBpz}_3)_2]^+$ , which forms in large quantities but can easily be separated. The structure and properties of this complex are presented and compared to the binuclear system elsewhere.<sup>17</sup> Recently, a complex similar to **1**,  $[\text{Fe}_2\text{O}(\text{O}_2\text{CCH}_3)_2(\text{TCN})_2]^{2+}$ , where TCN = 1,4,7-triazacyclononane, was reported.<sup>18</sup>

## Experimental Section

**Materials and Methods. Preparation of Compounds.** Potassium tri-1-pyrazolylborate ( $\text{KHBpz}_3$ ) was prepared by a literature method.<sup>19</sup>  $^{18}\text{O}$ -enriched (99%) water was purchased from Stohler Isotope Chemicals, Waltham, MA. All other reagents were obtained from commercial sources and used without further purification. Elemental analyses were performed by Galbraith Laboratories, Knoxville, TN, and by Atlantic Microlab Inc., Atlanta, GA.

**( $\mu$ -Oxo)bis( $\mu$ -acetato)bis(tri-1-pyrazolylborato)diiron(III),  $[\text{Fe}_2\text{O}(\text{O}_2\text{CCH}_3)_2(\text{HBpz}_3)_2]$  (**1**).** To a clear red-brown solution containing 10.00 g (18.71 mmol) of  $\text{Fe}(\text{ClO}_4)_3 \cdot 10\text{H}_2\text{O}$ , 5.09 g (37.40 mmol) of  $\text{Na}(\text{O}_2\text{C}-\text{CH}_3) \cdot 3\text{H}_2\text{O}$ , and 200 mL of  $\text{H}_2\text{O}$  (solution pH 2.3) was added with rapid stirring a solution of 4.72 g (18.72 mmol) of  $\text{KHBpz}_3$  in 100 mL of  $\text{H}_2\text{O}$ . A golden-brown solid precipitated immediately; however, with stirring the suspension took on a deep red appearance. After  $\sim 12$  h the mixture was filtered (filtrate pH 3.9) and the solid was dried under vacuum to afford 6.1 g of a red solid that was shown ( $^1\text{H}$  NMR, UV-vis) to contain both **1** and  $[\text{Fe}(\text{HBpz}_3)_2]^+$  salts. This solid was stirred with 30 mL of  $\text{CH}_3\text{CN}$  for several minutes, and the mixture was filtered. This first batch of crystalline solid was washed with  $2 \times 10$  mL of  $\text{CH}_3\text{CN}$ , and the combined  $\text{CH}_3\text{CN}$  filtrates were cooled to  $-20^\circ\text{C}$  for 4 h. The resulting green-brown microcrystals were collected by filtration, combined with the first crop, and dissolved in  $\text{CH}_2\text{Cl}_2$ . The slightly cloudy, green-brown solution was filtered to remove a small amount of colorless and red-brown solids. Removal of the solvent and drying in vacuo afforded 2.65 g (42.2%) of microcrystals of **1**. Further purification was achieved by recrystallization from  $\text{CH}_3\text{CN}$  (a saturated solution at room temperature was cooled to  $-20^\circ\text{C}$ ). Anal. Calcd for  $\text{Fe}_2\text{C}_{22}\text{H}_{26}\text{B}_2\text{N}_{12}\text{O}_5$

(**1**): C, 39.33; H, 3.90, N, 25.02; Fe, 16.63. Found: C, 39.22; H, 3.91; N, 25.18; Fe, 16.71.  $^1\text{H}$  NMR ( $\text{CDCl}_3$ , 295 K, 250 MHz)  $\delta$  (from  $\text{Me}_4\text{Si}$ ) -12.3 (br), -10.5 (br), -3.0 (br). UV-vis-near IR ( $\text{CHCl}_3$ )  $\lambda$  262 ( $\epsilon_{\text{Fe}}$  3380  $\text{cm}^{-1}\text{M}^{-1}$ ), 339 (4640), 358 (sh), 457 (505), 492 (460), 528 (sh), 695 (70), 995 (3.5). IR (KBr,  $\text{cm}^{-1}$ ) 3155, 3125, 2460 (B-H), 1560 ( $\nu_{\text{as}}$ , COO), 1503, 1427 ( $\nu_{\text{s}}$ , COO), 1402, 1391, 1352, 1309, 1215, 1116, 1094, 1070, 1051, 984, 926, 883, 819, 756, 716, 661, 620, 528, 360, 320, 245.  $\mu_{\text{eff}}$  ( $\text{CDCl}_3$ ) 1.71  $\mu_{\text{B}}$  per iron. Mass spectrum (by field desorption) 672 ( $\text{M}^+$ ), 612 ( $\text{M}^+ - (\text{O}_2\text{CCH}_3) - \text{H}$ ). Calcd formula weight 671.85.

The crystals used for X-ray diffraction experiments were found to contain four molecules of  $\text{CH}_3\text{CN}$  per binuclear complex (see below). Evidently, the solvent is lost readily under vacuum. Quantitative analysis of the optical and NMR spectra of the solvated and solvent-free compounds confirmed the presence of four acetonitrile molecules (3.8  $\text{CH}_3\text{CN}$  molecules per complex were detected by both methods).

Selectively deuterated **1** was required to facilitate assignment of the  $^1\text{H}$  NMR spectrum. Replacement of B-H with B-D and  $\text{CH}_3$  with  $\text{CD}_3$  was effected in the following manner. The complex  $[\text{Fe}_2\text{O}(\text{O}_2\text{CCH}_3)_2(\text{DBpz}_3)_2]$  was prepared from  $\text{Na}(\text{DBpz}_3)$ , obtained in the reaction of  $\text{NaBD}_4$  with pyrazole in the usual manner ( $\nu_{\text{B-D}} = 1826 \text{ cm}^{-1}$ ).<sup>19</sup> The synthesis of  $[\text{Fe}_2\text{O}(\text{O}_2\text{CCD}_3)_2(\text{HBpz}_3)_2]$  was accomplished by first generating  $\text{NaO}_2\text{CCD}_3$  in solution from  $\text{NaOH}$  and  $\text{DO}_2\text{CCD}_3$  and proceeding as for **1**.

**$^{18}\text{O}$ -Enriched  $[\text{Fe}_2^*\text{O}(\text{O}_2\text{CCH}_3)_2(\text{HBpz}_3)_2]$ .** Experiments showed that the bridging oxygen atom of **1** readily undergoes exchange with water in a two-phase system to provide highly enriched  $[\text{Fe}_2^{18}\text{O}(\text{O}_2\text{CCH}_3)_2(\text{HBpz}_3)_2]$  for study by resonance Raman spectroscopy (see below). To a solution of 54.5 mg (0.081 mmol) of **1** in 2 mL of  $\text{CH}_2\text{Cl}_2$  was added 100  $\mu\text{L}$  of 99% enriched  $^{18}\text{OH}_2$ . The mixture was stirred vigorously for  $\sim 20$  h. The  $\text{CH}_2\text{Cl}_2$  layer was removed by pipet, the solvent was stripped off in vacuo, and the resulting solid was dried under vacuum overnight. The product was characterized by its optical spectrum in chloroform. Analysis of its mass spectrum showed that  $^{18}\text{O}$  was incorporated only into the bridging position and that the sample was 85% enriched. Mass spectrum (by field desorption) 674 ( $\text{M}^+$ ), 614 ( $\text{M}^+ - (\text{O}_2\text{CCH}_3) - \text{H}$ ).

**( $\mu$ -Oxo)bis( $\mu$ -formato)bis(tri-1-pyrazolylborato)diiron(III),  $[\text{Fe}_2\text{O}(\text{O}_2\text{CH})_2(\text{HBpz}_3)_2]$  (**2**).** This compound was obtained in a manner analogous to that reported above for **1**. To a solution of 2.26 g (4.23 mmol) of  $\text{Fe}(\text{ClO}_4)_3 \cdot 10\text{H}_2\text{O}$  and 0.580 g (8.53 mmol) of  $\text{NaO}_2\text{CH}$  in 50 mL of  $\text{H}_2\text{O}$  was added a solution of 1.07 g (4.24 mmol) of  $\text{KHBpz}_3$  in 30 mL of  $\text{H}_2\text{O}$ . A brown precipitate formed immediately which turned slightly more reddish after 0.5 h when the suspension was filtered (filtrate pH 3.3). The solid was dried under vacuum to yield 1.40 g of a red-brown solid. In contrast to the preparative procedure of **1**, long ( $\sim 12$  h) reaction times resulted in very small yields of the desired complex with  $[\text{Fe}(\text{HBpz}_3)_2]^+$  as the only identified reaction product. The solid obtained after only 0.5 h of reaction time was stirred with 10 mL of  $\text{CH}_3\text{CN}$  for 10 min, and the mixture was filtered. The undissolved solid was washed with  $2 \times 4$  mL of  $\text{CH}_3\text{CN}$  and dried in the air. The combined filtrates were cooled to  $-20^\circ\text{C}$  for 4 h, and the green-brown needles which formed were filtered off, leaving a deep red filtrate. The two crops of product were combined and dried under vacuum to afford 0.53 g of product. This material was taken into  $\text{CH}_2\text{Cl}_2$  and filtered to remove a small amount of an insoluble red solid, and the solvent was removed by using a rotary evaporator. Drying under vacuum gave 0.50 g (37%) of **2**. As with **1**, further purification was achieved by recrystallization from a saturated acetonitrile solution formed at room temperature and slowly cooled to  $-20^\circ\text{C}$ . Anal. Calcd for  $\text{Fe}_2\text{C}_{20}\text{H}_{22}\text{B}_2\text{N}_{12}\text{O}_5$  (**2**): C, 37.31; H, 3.44; N, 26.11; formula weight 643.79. Found: C, 37.11; H, 3.45; N, 26.08. When obtained from  $\text{CH}_3\text{CN}$  solution, **2** crystallizes with four  $\text{CH}_3\text{CN}$  molecules of solution (see X-ray analysis) which are readily lost from the powdered solid under vacuum.  $^1\text{H}$  NMR ( $\text{CDCl}_3$ , 295 K) -12.4 (br), -9.1 (v br), -2.9 (br). UV-vis ( $\text{CHCl}_3$ )  $\lambda$  262 ( $\epsilon_{\text{Fe}}$  3250  $\text{cm}^{-1}\text{M}^{-1}$ ), 342 (5110), 460 (535), 489 (480),  $\sim 530$  (sh), 692 (69). IR (KBr,  $\text{cm}^{-1}$ ) 3155, 3130, 2845, 2830, 2465 (B-H), 1594, 1503, 1404, 1385, 1362, 1357, 1308, 1214, 1118, 1071, 1052, 985, 925, 885, 819, 764, 713, 663, 616, 523, 355 (br), 320 (br), 242.  $\mu_{\text{eff}}$  ( $\text{CDCl}_3$ ) 1.72  $\mu_{\text{B}}$  per iron. Mass spectrum (fast atom bombardment (FAB)) 644 ( $\text{M}^+$ ), 645 ( $\text{MH}^+$ ).

**( $\mu$ -Oxo)bis( $\mu$ -benzoato)bis(tri-1-pyrazolylborato)diiron(III),  $[\text{Fe}_2\text{O}(\text{O}_2\text{CC}_6\text{H}_5)_2(\text{HBpz}_3)_2]$  (**3**).** It was not possible to obtain **3** from aqueous solution following the procedure given above for **1** and **2**. The only identified product obtained from the heterogeneous mixture of reactants was  $[\text{Fe}(\text{HBpz}_3)_2]^+$ . An alternative route was therefore devised which utilizes a preformed ( $\mu$ -oxo)diiron(III) core. To a solution of 1.50 g (2.50 mmol) of  $(\text{Et}_4\text{N})_2(\text{Fe}_2\text{OCl}_6)^{17}$  in 25 mL of  $\text{CH}_3\text{CN}$  was added 0.720 g (5.00 mmol) of  $\text{NaO}_2\text{CPh}$  with vigorous stirring. After 15 min, 1.26 g (5.00 mmol) of  $\text{KHBpz}_3$  in 20 mL of  $\text{CH}_3\text{CN}$  was added to the inhomogeneous red-brown reaction mixture. The suspension quickly became an olive-green color. After 20 min the mixture was filtered to afford a light colored precipitate and an olive-green filtrate which was shown from

(11) (a) Paul, R. C.; Narula, R. C.; Kaur, S.; Vasisht, S. K. *Trans. Met. Chem.* **1976**, *1*, 284-288. (b) Paul, R. C.; Narula, R. C.; Vasisht, S. K. *Ibid.* **1978**, *3*, 35-38. (c) Vasisht, S. K.; Narula, R. C. *Ibid.* **1982**, *7*, 95-96.

(12) Holm, R. H.; Ibers, J. A. *Science* **1980**, *209*, 223-235.

(13) Hagen, K. S.; Watson, A. D.; Holm, R. H. *J. Am. Chem. Soc.* **1983**, *105*, 3905-3913.

(14) Thompson, J. S.; Marks, T. J.; Ibers, J. A. *J. Am. Chem. Soc.* **1979**, *101*, 4180-4192.

(15) Armstrong, W. H.; Lippard, S. J. *J. Am. Chem. Soc.* **1983**, *105*, 4837-4838.

(16) Armstrong, W. H.; Lippard, S. J.; Co, M. S.; Hodgson, K. O.; Smith, J. L.; Hendrickson, W. A., to be submitted for publication.

(17) Armstrong, W. A.; Lippard, S. J., to be submitted for publication.

(18) Wiegardt, K.; Pohl, K.; Gebert, W. *Angew. Chem., Int. Ed. Engl.* **1983**, *22*, 727.

(19) Trofimenko, S. *Inorg. Synth.* **1970**, *12*, 99-109.

its optical spectrum to contain almost pure **3** (no detectable  $\text{Fe}(\text{HBpz}_3)_2^+$ ). Addition of 200 mL of  $\text{H}_2\text{O}$  precipitated a green solid which was collected by filtration after 1 h of stirring and dried under vacuum to afford 1.86 g (94%) of product. This solid was dissolved in  $\text{CH}_2\text{Cl}_2$  and filtered, and the solvent was evaporated until a dark green oil was obtained. Addition of 30 mL of acetone and partial evaporation led to crystallization of **3**. Occasionally several acetone addition and complete evaporation steps must be repeated to initiate crystallization. The green solid was filtered and washed with ~5–10 mL of acetone and dried under vacuum to yield 1.42 g (71.5%) of pure **3**. Anal. Calcd for  $\text{C}_{32}\text{H}_{30}\text{N}_{12}\text{O}_3\text{B}_2\text{Fe}_2$  (**3**): C, 48.29; H, 3.80; N, 21.11; formula weight 795.99. Found: C, 48.02; H, 4.05; N, 20.77.  $^1\text{H}$  NMR ( $\text{CDCl}_3$ , 295 K)  $\delta$  -13.2 (br), ca. -10.5 (v br), -8.68 (meta), -6.90 (para), -3.0. UV-vis ( $\text{CHCl}_3$ )  $\lambda$  265 ( $\epsilon_{\text{Fe}}$  5750  $\text{cm}^{-1}\text{M}^{-1}$ ), 336 (4500), ~360 (sh), 455 (480), 490 (430), ~525 (sh), 691 (65). IR (KBr,  $\text{cm}^{-1}$ ) 3145, 3130, 2480 (B-H), 1595, 1547, 1407, 1313, 1215, 1113, 1051, 883, 839, 818, 795, 763, 724, 717, 678, 662, 620, 534, 470, 456, 360, 340, 300, 286, 260, 234. Mass spectrum (FAB) 796 ( $\text{M}^+$ ), 797 ( $\text{MH}^+$ ).

**Collection and Reduction of X-ray Data for  $[\text{Fe}_2\text{O}(\text{O}_2\text{CCH}_3)_2(\text{HBpz}_3)_2]\cdot 4\text{CH}_3\text{CN}$  (**1**·4 $\text{CH}_3\text{CN}$ ).** Plate-like crystals of **1** appear either green or brown by transmitted light through a polarizing filter depending on the viewing angle. The crystal used for data collection was obtained by slow evaporation of an acetonitrile solution of **1**. Its shape was that of a truncated square pyramid. The crystal was sealed in a glass capillary to prevent solvent loss, which occurs rapidly in air. The crystal quality was found to be acceptable on the basis of  $\omega$  scans of several low-angle reflections ( $\Delta\omega_{1/2} \approx 0.2^\circ$ ). The diffractometer data and Weissenberg photographs showed the crystal to belong to the monoclinic system with systematic absences  $h0l$ ,  $h + l = 2n + 1$ , and  $0k0$ ,  $k = 2n + 1$ , consistent with space group  $P2_1/n$  ( $C_{2h}^2$ , No. 14<sup>20a</sup> in a nonstandard setting). The choice of space group was confirmed by the successful solution and refinement of the structure. Data collection and reduction were carried out by previously described procedures,<sup>21</sup> details of which are presented in Table I.

**$[\text{Fe}_2\text{O}(\text{O}_2\text{CH})_2(\text{HBpz}_3)_2]\cdot 4\text{CH}_3\text{CN}$  (**2**·4 $\text{CH}_3\text{CN}$ ).** The crystal used in the diffraction study was grown from an acetonitrile solution of **2** by slow evaporation. These crystals also lose solvent very readily, and thus it was necessary to seal the crystal in a glass capillary and to carry out the X-ray experiments at low temperature ( $-25 \pm 2^\circ\text{C}$ ). At one point during the data collection, solvent loss caused a marked decrease in diffracted intensities (see Table I). Several low-angle  $\omega$  scans showed the crystal quality to be acceptable ( $\Delta\omega_{1/2} \approx 0.15^\circ$ ). The crystal belongs to the orthorhombic system, and the space group was determined to be either  $Pnma$  ( $D_{2h}^{16}$ , No. 62) or  $Pn2_1a$  ( $C_{2h}^2$ , No. 33 in a nonstandard setting)<sup>20b</sup> from the systematic absences  $0kl$ ,  $k + l = 2n$ , and  $hk0$ ,  $h = 2n$ . The former choice, supported by statistical tests,<sup>22</sup> was confirmed by solution and refinement of the structure. Further details of the data collection and reduction are given in Table I.

**Structure Solution and Refinement.  $[\text{Fe}_2\text{O}(\text{O}_2\text{CCH}_3)_2(\text{HBpz}_3)_2]\cdot 4\text{CH}_3\text{CN}$  (**1**·4 $\text{CH}_3\text{CN}$ ).** The positions of the two unique Fe atoms were located from a Patterson map. All remaining non-hydrogen atoms were revealed in subsequent difference Fourier maps. The structure was refined by using anisotropic thermal parameters for all non-hydrogen atoms. Neutral atom scattering factors and anomalous dispersion corrections for non-hydrogen atoms were obtained from ref 23, and hydrogen atom scattering factors were taken from ref 24. All hydrogen atoms (except HB1 and HB2) were placed at calculated positions,  $d(\text{C-H}) = 0.95 \text{ \AA}$ , constrained to "ride" on the carbon atoms to which they are attached<sup>25</sup> toward the end of the refinement, and fixed in the final refinement cycles. Positions of the hydrogen atoms bound to B1 and B2 were allowed to refine independently. A common isotropic thermal parameter was used for each of the following atom groups: (1) pyrazolyl ring hydrogens, (2) acetate methyl hydrogens, and (3) acetonitrile H atoms. Least-squares refinement<sup>25</sup> converged to the  $R$  indices listed in Table I. The function minimized during refinement was  $\sum w(|F_o| - |F_c|)^2$ , where  $w = 1.1356/[\sigma^2(F_o) + 0.000625(F_o)^2]$ . The largest ratio of parameter shift to estimated standard deviation in the final cycle of refinement was  $<0.05$ , and the largest peak and the final difference Fourier map was  $\sim 0.5 \text{ e\AA}^{-3}$ . Final positional parameters are presented in Table II, and a list of interatomic distances and angles is given in Table IV. A listing of observed and calculated structure factors is supplied in Table S1 (supplementary material), and the final thermal parameters for all non-hydrogen atoms and for HB1 and HB2 are given in Table S3.

(20) "International Tables for X-ray Crystallography"; 3rd ed.; Kynoch Press: Birmingham, England, 1973; Vol. I: (a) p 99; (b) pp 119 and 151.

(21) Silverman, L. D.; Dewar, J. C.; Giandomenico, C. M.; Lippard, S. J. *Inorg. Chem.* **1980**, *19*, 3379–3383.

(22) Germain, G.; Main, P.; Woolfson, M. M. *Acta Crystallogr., Sect. A* **1971**, *A27*, 368–376.

**Table I.** Experimental Details of the X-ray Diffraction Studies of  $[\text{Fe}_2\text{O}(\text{O}_2\text{CR})_2(\text{HBpz}_3)_2]\cdot 4\text{CH}_3\text{CN}$  ( $\text{R} = \text{CH}_3$ , **1**·4 $\text{CH}_3\text{CN}$ ;  $\text{R} = \text{H}$ , **2**·4 $\text{CH}_3\text{CN}$ )

(A) Crystal Parameters <sup>a</sup>					
	<b>1</b> <sup>b</sup>	<b>2</b> <sup>c</sup>		<b>1</b>	<b>2</b>
$a$ , $\text{Å}$	13.236 (1)	15.515 (2)	space group	$P2_1/n$	$Pnma$
$b$ , $\text{Å}$	15.414 (2)	19.764 (3)	$Z$	4	4
$c$ , $\text{Å}$	21.697 (2)	12.720 (1)	$\rho$ (calcd), $\text{g cm}^{-3}$	1.313	1.376
$\beta$ , deg	107.26 (1)	90	$\rho$ (obsd), <sup>d</sup> $\text{g cm}^{-3}$	1.319 (9)	1.38 (1)
vol, $\text{Å}^3$	4227.3	3900.3	mol wt	836.06	808.00

(B) Measurement and Treatment of Intensity Data<sup>e</sup>  
instrument: Enraf-Nonius CAD-4F  $\kappa$ -geometry diffractometer;  
radiation: Mo  $K\alpha$  ( $\lambda_\alpha = 0.71073 \text{ \AA}$ ) graphite monochromatized

	<b>1</b>	<b>2</b>
standards	(2,5,8) (0,6,5) (0,6,5), monitored every 9000 s, varied randomly with no overall decay in the average of the three standards	(10,1,3) (6,6,6) (3,4,8), monitored every 7200 s, step-function-like decay of ~13% was corrected <sup>f</sup>
no. of reflections collected exclusive of systematic absences	10121 [ $3^\circ \leq 2\theta \leq 55^\circ$ ( $+h,+k,\pm l$ )]	3969 [ $3^\circ \leq 2\theta \leq 52^\circ$ ( $+h,+k,+l$ )] <sup>g</sup>
abs corr		
crystal size, mm	0.30 × 0.30 × 0.40	
linear abs coeff, $\text{cm}^{-1}$	7.36	7.81
transmission factors	0.78–0.81 <sup>h</sup>	0.76–0.83 <sup>i</sup>
crystal faces	{001}; {110}	$i$
average, $R_{\text{av}}$ <sup>e</sup>	0.050	0.056
no. of reflections after averaging	9676	3935

(C) Final Model in Least-Squares Refinement<sup>e</sup>

	<b>1</b>	<b>2</b>
final $R$ values <sup>j</sup>	$R_1 = 0.040$ $R_2 = 0.048$	$R_1 = 0.038$ $R_2 = 0.052$
no. of observations	5277 [ $F_o > 4\sigma(F_o)$ ]	2597 [ $F_o > 6\sigma(F_o)$ ]
no. of variable parameters	505	280

<sup>a</sup> From a least-squares fit to the setting angles of 25 reflections with  $2\theta \geq 22^\circ$  for **1** and  $2\theta \geq 23^\circ$  for **2**. <sup>b</sup> Unit cell parameters and data collection at  $24 \pm 1^\circ\text{C}$ . <sup>c</sup> All measurements were carried out at  $-25 \pm 2^\circ\text{C}$ . <sup>d</sup> By suspension in a mixture of  $\text{CCl}_4$  and heptane. <sup>e</sup> See ref 21 for further details. <sup>f</sup> After collecting data in the region  $3^\circ \leq 2\theta \leq 36^\circ$ , the crystal was allowed to warm to room temperature for ca. 1 h which presumably caused loss of solvent and the resulting decline in crystal quality. <sup>g</sup> A set of data with  $3^\circ \leq 2\theta \leq 20^\circ$  ( $\pm h,k,\pm l$ ) was also collected to confirm the crystal symmetry. <sup>h</sup> Absorption corrections were performed with the Wehe-Busing-Levy ORABS program. <sup>i</sup> No absorption correction was applied. <sup>j</sup>  $R_1 = \sum(|F_o| - |F_c|)/\sum|F_o|$ ;  $R_2 = [\sum w(|F_o|^2 - |F_c|^2)/\sum w|F_o|^2]^{1/2}$ .

Positional and thermal parameters for fixed hydrogen atoms are given in Table S4.

**$[\text{Fe}_2\text{O}(\text{O}_2\text{CH})_2(\text{HBpz}_3)_2]\cdot 4\text{CH}_3\text{CN}$  (**2**·4 $\text{CH}_3\text{CN}$ ).** The two unique Fe atom positions were located by direct methods using MULTAN.<sup>22</sup> Both Fe

**Table II.** Final Positional Parameters for  $[\text{Fe}_2\text{O}(\text{O}_2\text{CCH}_3)_2(\text{HBpz}_3)_2]\cdot 4\text{CH}_3\text{CN}$  ( $1\cdot 4\text{CH}_3\text{CN}$ )<sup>a-d</sup>

ATOM	X	Y	Z
Fe1	-0.07475(3)	0.04133(3)	0.24925(2)
Fe2	0.11183(3)	0.16799(3)	0.24973(2)
O	0.05765(14)	0.06162(11)	0.24924(10)
O11	-0.07488(18)	0.12558(14)	0.32174(11)
O12	-0.14587(16)	0.13021(14)	0.18029(11)
O21	0.05520(19)	0.21766(14)	0.32066(12)
O22	-0.01339(17)	0.22048(14)	0.18095(12)
N11	-0.0380(2)	-0.06477(16)	0.31679(13)
N12	-0.23769(19)	0.01067(16)	0.24797(14)
N13	-0.1036(2)	-0.06119(16)	0.17833(13)
N14	-0.0979(2)	-0.13914(16)	0.30620(14)
N15	-0.27126(19)	-0.07341(16)	0.24613(14)
N16	-0.1540(2)	-0.13591(17)	0.18623(14)
N21	0.2616(2)	0.13979(17)	0.31927(13)
N22	0.1845(2)	0.29458(16)	0.24969(13)
N23	0.19265(19)	0.14162(16)	0.17931(12)
N24	0.3541(2)	0.16505(18)	0.30926(14)
N25	0.2873(2)	0.30202(16)	0.25058(13)
N26	0.2950(2)	0.16689(16)	0.18912(13)
N3	0.5163(5)	0.1200(4)	0.0503(3)
N4	0.9079(5)	0.0955(4)	0.0095(3)
N5	0.1810(5)	0.3539(5)	-0.0142(3)
N6	0.3371(8)	0.5915(6)	0.0086(3)
C11	0.0391(3)	-0.0772(2)	0.37140(17)
C12	0.0305(3)	-0.1576(3)	0.39727(19)
C13	-0.0566(3)	-0.1945(2)	0.3549(2)
C14	-0.3210(3)	0.0595(2)	0.2468(2)
C15	-0.4077(3)	0.0084(3)	0.2440(2)
C16	-0.3724(3)	-0.0748(3)	0.2437(2)
C17	-0.0779(3)	-0.0699(2)	0.12431(18)
C18	-0.1106(3)	-0.1495(3)	0.09617(19)
C19	-0.1586(3)	-0.1892(2)	0.1365(2)
C21	0.2871(3)	0.0969(3)	0.37479(19)
C22	0.3954(4)	0.0939(3)	0.4009(2)
C23	0.4345(3)	0.1375(3)	0.3588(2)
C24	0.1488(3)	0.3750(2)	0.2499(2)
C25	0.2261(3)	0.4342(2)	0.2507(2)
C26	0.3124(3)	0.3869(2)	0.25096(18)
C27	0.1629(3)	0.1009(2)	0.12236(17)
C28	0.2459(4)	0.0992(3)	0.0951(2)
C29	0.3264(3)	0.1413(3)	0.1383(2)
C31	-0.0155(3)	0.1894(2)	0.34313(16)
C32	-0.0324(4)	0.2372(3)	0.3996(2)
C41	-0.1080(3)	0.1956(2)	0.16029(15)
C42	-0.1816(3)	0.2491(3)	0.10836(19)
C51	0.5799(4)	0.0688(4)	0.0594(3)
C52	0.6593(4)	0.0022(4)	0.0729(3)
C61	0.8551(4)	0.1294(4)	-0.0323(2)
C62	0.7855(7)	0.1686(5)	-0.0851(3)
C71	0.1554(5)	0.3448(4)	0.0298(3)
C72	0.1179(7)	0.3338(4)	0.0831(3)
C81	0.3212(8)	0.5441(5)	-0.0337(3)
C82	0.3108(7)	0.4914(5)	-0.0825(4)
H1	-0.1932(3)	-0.1473(2)	0.2455(2)
H2	0.3523(3)	0.2193(3)	0.2497(2)
HB1	-0.233(2)	-0.2099(19)	0.2461(13)
HB2	0.424(2)	0.2334(20)	0.2521(14)

<sup>a</sup> Atoms are labeled as shown in Figure 1. <sup>b</sup> Positions are given for all non-hydrogen atoms and for the hydrogen atoms that were refined. <sup>c</sup> The hydrogen atoms are labeled according to the boron atoms to which they are attached. <sup>d</sup> Estimated standard deviations, in parentheses, occur in the last significant figure(s) for each parameter.

atoms lie in the plane  $y = 1/4$ . Subsequent difference Fourier maps revealed the positions of all remaining non-hydrogen atoms. As with  $1\cdot 4\text{CH}_3\text{CN}$ , the structure was refined with anisotropic thermal parameters for all non-hydrogen atoms. The positions of the hydrogen atoms bonded to boron or to the formate carbon atom were allowed to refine independently while the pyrazolyl ring and methyl hydrogen atoms were placed at calculated positions and constrained to "ride" on their bonded carbon atoms. A common isotropic thermal parameter was refined for each of the following H-atom types: (1) pyrazolyl ring and (2) acetonitrile  $\text{CH}_3$ . Full-matrix least-squares refinement converged to the  $R$  values shown in Table I. The weighting function used in the refinement was  $w = 1.3823/[\sigma^2(F_o) + 0.000625(F_o^2)]$ , and the maximum parameter shift in the final cycle of refinement was  $0.02\sigma$ . The largest residual peak in the final difference Fourier map was  $\sim 0.33 \text{ e}\text{\AA}^{-3}$ . The final atomic positional parameters are presented in Table III, and a list of interatomic distances and angles is given in Table IV. Observed and calculated structure factors are given in Table S2, and final thermal parameters for all non-hydrogen atoms and HC31, HB1, and HB2 are supplied in Table S5. Final positional and thermal parameters for the nonrefined hydrogen atoms are given in Table S6.

**Physical Measurements. Electrochemistry.** Cyclic voltammetry (CV) experiments were performed with a Princeton Applied Research (PAR) Model 173 potentiostat and a Model 175 universal programmer. CV results for scan rates less than  $500 \text{ mV s}^{-1}$  were recorded on a Houston Instruments Model 2000 X-Y recorder while fast scan ( $> 500 \text{ mV s}^{-1}$ ) CV data were recorded with use of a Tektronix 564 storage oscilloscope equipped with a Polaroid camera. Experiments were carried out in acetonitrile with use of  $0.1 \text{ M}$  tetra-*n*-butylammonium perchlorate (TBAP),  $0.1 \text{ M}$  tetra-*n*-butylammonium acetate (TBAA), or  $0.2 \text{ M}$   $\text{LiClO}_4$  as the supporting electrolyte. In methylene chloride ( $\text{CH}_2\text{Cl}_2$ ) and dimethylformamide (DMF) solvents, TBAP was used as the sup-

**Table III.** Final Positional Parameters for  $[\text{Fe}_2\text{O}(\text{O}_2\text{CH})_2(\text{HBpz}_3)_2]\cdot 4\text{CH}_3\text{CN}$  ( $2\cdot 4\text{CH}_3\text{CN}$ )<sup>a</sup>

ATOM	X	Y	Z
Fe1	0.10995(4)	0.2500	-0.11142(5)
Fe2	0.23610(4)	0.2500	0.08439(5)
O	0.21414(17)	0.2500	-0.0534(2)
O11	0.05837(16)	0.32261(15)	-0.01469(18)
O21	0.14844(15)	0.32354(12)	0.12342(17)
N11	0.13701(18)	0.32308(14)	-0.2305(2)
N12	-0.0155(3)	0.2500	-0.1864(3)
N14	0.10983(18)	0.31289(15)	-0.3316(2)
N15	-0.0239(2)	0.2500	-0.2930(3)
N21	0.33835(17)	0.32344(15)	0.0806(2)
N22	0.2650(2)	0.2500	0.2530(3)
N24	0.41231(17)	0.31329(16)	0.1369(2)
N25	0.3482(2)	0.2500	0.2862(3)
N3	0.1481(4)	0.0341(3)	0.3754(4)
N4	0.3735(6)	0.0108(5)	0.5384(8)
C11	0.1801(3)	0.3808(2)	-0.2310(4)
C12	0.1810(3)	0.4090(2)	-0.3309(4)
C13	0.1356(3)	0.3651(2)	-0.3910(3)
C14	-0.0955(4)	0.2500	-0.1513(5)
C15	-0.1541(4)	0.2500	-0.2308(6)
C16	-0.1085(3)	0.2500	-0.3182(5)
C21	0.3463(3)	0.3821(2)	0.0312(3)
C22	0.4265(3)	0.4115(2)	0.0553(4)
C23	0.4654(3)	0.3661(2)	0.1225(3)
C24	0.2170(3)	0.2500	0.3389(4)
C25	0.2673(4)	0.2500	0.4278(4)
C26	0.3496(4)	0.2500	0.3908(4)
C31	0.0858(3)	0.3442(2)	0.0713(3)
C41	0.2114(4)	0.0522(3)	0.3464(4)
C42	0.2935(5)	0.0768(3)	0.3087(6)
C51	0.4097(6)	0.0360(5)	0.6005(8)
C52	0.4534(6)	0.0655(5)	0.6839(7)
H1	0.0567(4)	0.2500	-0.3591(4)
H2	0.4223(4)	0.2500	0.2051(5)
HC31	0.055(2)	0.3808(18)	0.104(2)
HB1	0.039(3)	0.2500	-0.442(4)
HB2	0.490(3)	0.2500	0.247(3)

<sup>a</sup> Atoms are labeled as shown in Figure 2. The hydrogen atoms are labeled according to the boron and carbon atoms to which they are attached. See footnotes *b* and *d* in Table II.

porting electrolyte. Acetonitrile (Photrex grade from J. T. Baker Chemical Co.) was either distilled from  $\text{CaH}_2$  or used directly from the bottle. DMF was stored over KOH and freshly distilled from BaO. Methanol was distilled from  $\text{Mg}(\text{OMe})_2$ . TBAP and TBAA were each recrystallized three times before use. A three-electrode system was employed, consisting of a platinum bead or glassy carbon working electrode, a platinum wire auxiliary electrode, and a PAR saturated calomel (SCE) reference electrode separated from the bulk solution by a bridge fitted with the working solvent and supporting electrolyte. Vycor plugs were used at the SCE/bridge and bridge/bulk solution junctions. Measurements were made at room temperature ( $25^\circ\text{C}$ ) under nitrogen. The electrode performance was monitored by measuring the  $\text{Fe}(\text{II})/\text{Fe}(\text{III})$  couple of ferrocene in the working solution ( $\sim 1 \text{ mg}/3 \text{ mL}$  of solution), although measurements of  $\text{Fe}(\text{HBpz}_3)_2^{+17}$  proved to be equally good tests for the integrity of the electrode surface.

**Raman Spectroscopy.** Raman spectra were recorded by using a Spex double monochromator equipped with a cooled RCA 31034 photomultiplier tube and photon counting electronics. Spectra were recorded on a Linear Instruments Corp. chart recorder. Laser excitations at 453 to 514 nm with 30–60 mW of power incident at the sample were obtained by using a Coherent Radiation Model 52 tunable argon ion laser. A Coherent Radiation CR-599 Dye laser using rhodamine 6G or rhodamine 560 and a Model 591 utility module with the CR52 argon laser set for all lines to pump the dye were used to obtain frequencies between 540 and 624 nm with 20–55 mW of power incident at the sample. A Coherent Radiation Model CR18 tunable argon ion laser equipped with UV optics was used for 364-nm radiation with 100 mW incident at the sample. Slits were set to 200/250/200  $\mu\text{m}$  in all spectra. A backscattering geometry was used with samples contained in spinning 5-mm NMR tubes when liquid samples were used or spinning sealed capillaries when solid samples were irradiated.

A sample of **1** was prepared by nearly saturating 0.5 mL of  $\text{CH}_2\text{Cl}_2$  with the compound and sealing the tube. This sample was used for all solution Raman spectra of **1**. Compound **1** was stable in solution during excitation at all wavelengths. Relative peak areas were estimated by cutting and weighing the recorder tracings. The excitation profile of a given peak was determined from the ratio of its area to that of the symmetrical  $\text{CCl}_2$  stretching vibration at  $703 \text{ cm}^{-1}$  of the methylene chloride solvent. The profile obtained was identical with that obtained by using peak heights instead of areas. Peak height ratios were therefore used for the final excitation profile. Corrections for the sample absorption<sup>26</sup> were found to be within experimental error and were consequently not made.

**Mössbauer Spectroscopy.** Mössbauer spectra were recorded by using a conventional constant acceleration spectrometer equipped with a temperature controller maintaining temperatures within  $\pm 0.1 \text{ K}$  and a  $\text{Nb}_3\text{Sn}$



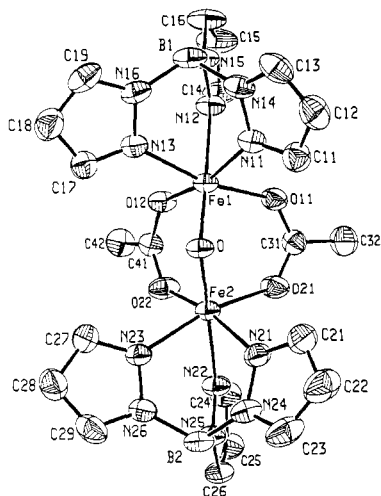


**Figure 1.** Structure of **1** showing the 40% probability thermal ellipsoids and the atom-labeling scheme.

to favor the formation of  $[\text{Fe}(\text{HBpz}_3)_2]^+$ .

Although the "self-assembly" synthesis is effective for the formate, acetate, and propionate (unpublished results) derivatives, to prepare the benzoate analogue, it was necessary to use  $\text{Fe}_2\text{OCl}_6^{2-}$  as a starting material in nonaqueous reaction mixtures. Yet another route, involving isolation of the insoluble "(TCN) $\text{FeCl}_3$ ", TCN = 1,4,7-triazacyclononane, intermediate, has been employed to synthesize the analogous complex  $[\text{Fe}_2\text{O}(\text{O}_2\text{CCH}_3)_2(\text{TCN})_2]^{2+}$ .<sup>18</sup> The existence of these different ( $\mu$ -oxo)bis( $\mu$ -carboxylato)diiron(III) complexes underscores the intrinsic stability of the " $\text{Fe}_2\text{O}(\text{O}_2\text{CR})_2$ " core found in hemerythrin and possibly other nonheme iron proteins.

In order to facilitate the assignment of infrared, Raman, and NMR spectra, several isotopically substituted derivatives of **1** were required. Deuterated analogues were obtained by using  $\text{DBpz}_3^-$  in place of  $\text{HBpz}_3^-$  in one case and  $\text{O}_2\text{CCD}_3^-$  for  $\text{O}_2\text{CCH}_3^-$  in another. Exchange of the bridging oxo atom proved to be a facile process and was quantitatively achieved by stirring a  $\text{CH}_2\text{Cl}_2$  solution of **1** with  $^{18}\text{OH}_2$  for several hours. With use of infrared spectroscopy it was found that this exchange was 30% complete after 7 min. The facile exchange of  $^{18}\text{O}$  into the ( $\mu$ -oxo)diiron(III) core is discussed in more detail below.

**Description of the Structures.** Although it is not crystallographically imposed, **1** has nearly perfect  $C_{2v}$  symmetry (Figure 1). The asymmetric unit consists of the neutral, binuclear complex  $[\text{Fe}_2\text{O}(\text{O}_2\text{CCH}_3)_2(\text{HBpz}_3)_2]$  and four  $\text{CH}_3\text{CN}$  molecules of crystallization. A higher pseudosymmetry is indicated by the presence of an approximate mirror plane containing 15 atoms (2 Fe, oxo, 2 B, 2 pz rings), all of which have nearly the same  $z$  coordinates (all close to  $1/4$ ). The shapes of the thermal ellipsoids of the atoms lying on this pseudomirror plane, and those related by it, also reflect this pseudosymmetry (Figure 1). The largest deviation from the best least-squares plane defined by the 15 atoms is 0.047 Å, for atom Fe1. The largest  $\Delta$ , where  $\Delta$  is defined as the difference in the distances of pseudo-mirror-related atoms from the  $z = 1/4$  plane, is 0.18 Å, for atoms C13 and C19. In the formate analogue, the  $[\text{Fe}_2\text{O}(\text{O}_2\text{CH})_2(\text{HBpz}_3)_2]$  complex lies on a crystallographically required mirror plane (Figure 2) and the space group symmetry is higher (orthorhombic  $Pnma$  vs. monoclinic  $P2_1/n$  for 1- $4\text{CH}_3\text{CN}$ ). The two crystalline forms are related by minor differences in crystal packing originating no doubt from the slightly different steric requirements of the bridging acetate and formate ligands. The shortest intermolecular contacts are 2.26 Å [ $\text{H}(\text{C}16)\cdots\text{H}(\text{C}24)$ ] in **1** and 1.86 Å [ $\text{H}(\text{C}14)\cdots\text{H}(\text{C}26)$ ] in **2**.

The structures of **1** and **2**, shown in Figures 1 and 2, respectively, are composed of two six-coordinate iron atoms bridged by a single oxygen atom and two bidentate acetate groups and capped by tridentate tri-1-pyrazolylborate ligands. Both iron atoms are surrounded by a distorted octahedral array of ligands. Three

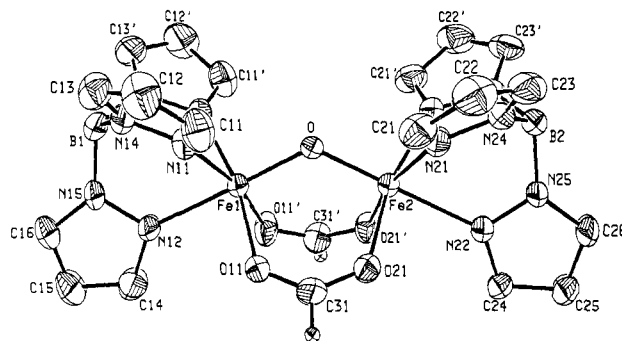


**Figure 2.** Structure of **2** showing the 40% probability thermal ellipsoids and the atom labels; primed and unprimed atoms are related by a crystallographically required mirror plane.

pyrazole nitrogen atoms occupy the coordination faces external to the diiron core, and three oxygen atoms are the face internal to the bridged diiron unit. Angles with idealized values of  $90^\circ$  range from  $81.7^\circ$  [ $\text{N}(22)\text{-Fe}(2)\text{-N}(23)$ ] to  $97.0^\circ$  [ $\text{O-Fe}(2)\text{-O}(22)$ ]. A major factor in the distortion from the octahedral values is the steric constraint of the tri-1-pyrazolylborate ligand. This constraint is relieved in the low-spin  $\text{Fe}(\text{HBpz}_3)_2^+$  structure<sup>17</sup> ( $\langle \text{N-Fe-N} \rangle = 88.5^\circ$ ), where the Fe-N bond lengths are shorter [ $\text{Fe}(\text{HBpz}_3)_2^+$ ,  $\langle \text{Fe-N} \rangle = 1.957$  Å; **1** and **2**,  $\langle \text{Fe-N} \rangle = 2.160$  Å] than in the high-spin (vide infra) iron complexes **1** and **2**. Movement of the relatively rigid tridentate ligand away from the iron center in **1** or **2** vs.  $[\text{Fe}(\text{HBpz}_3)_2]^+$  gives rise to significantly smaller N-Fe-N angles. The principal region of ligand flexibility appears to be in the N-B-N angles, which have increased markedly in **1** and **2** relative to the  $[\text{Fe}(\text{HBpz}_3)_2]^+$  cation. In **1** and **2** the tridentate ligand opens up as much as possible to accommodate the longer Fe-N bond distances [ $[\text{Fe}(\text{HBpz}_3)_2]^+$ ,  $\langle \text{N-B-N} \rangle = 105.7^\circ$ ; **1**, **2**,  $\langle \text{N-B-N} \rangle = 108.4^\circ$ ]. The mean N-B-N angles in **1** and **2** are similar to those in other complexes of  $\text{HBpz}_3^-$ , discussed elsewhere,<sup>17</sup> which supports the contention that the corresponding angles in  $[\text{Fe}(\text{HBpz}_3)_2]^+$  are unusually small.<sup>17</sup> Other ligand structural parameters in **1** and **2**,  $\langle \text{B-N} \rangle$  (1.53 Å),  $\langle \text{N-N} \rangle$  (1.37 Å),  $\langle \text{N-C} \rangle$  (1.33 Å), and  $\langle \text{C-C} \rangle$  (1.37 Å), are typical of the tri-1-pyrazolylborate ligand in its transition-metal complexes.<sup>17</sup>

The Fe-N and Fe-O (acetate) distances in **1** and **2** are in accord with values for other high-spin iron(III) complexes. For example, in two complexes that have the  $\text{N}_4\text{O}_2$  donor set around a central high-spin iron(III) atom,  $[\text{Fe}(\text{acacCl})_2\text{trien}](\text{PF}_6)$ <sup>18</sup> and  $[\text{Fe}(\text{acac})_2\text{trien}](\text{PF}_6)$ ,<sup>18</sup> the mean Fe-N (2.135, 2.136 Å, respectively) and Fe-O (1.908, 1.930 Å) bond lengths may be compared with the corresponding distances in **1** and **2**,  $\langle \text{Fe-N} \rangle = 2.160$  Å,  $\langle \text{Fe-O}(\text{acetate}) \rangle = 2.043$  Å,  $\langle \text{Fe-O}(\text{formate}) \rangle = 2.053$  Å. The mean Fe-N distance (2.172 Å) in the high-spin iron(II) complex,  $[\text{Fe}(\text{HB}(3,5\text{-Me}_2\text{pz})_2)_2]$ ,<sup>29</sup> is close to that of **1** and **2**. The average Fe-N bond lengths in **1** and **2** may also be compared to those in other oxo-bridged binuclear iron complexes:  $\text{enH}_2\{[\text{FeHEDTA}]_2\text{O}\}\cdot 6\text{H}_2\text{O}$ <sup>30</sup> (2.25 Å),  $\{[\text{FeB}(\text{H}_2\text{O})_2\text{O}](\text{ClO}_4)_4\}$ <sup>31</sup> (2.2 Å),  $[\text{Fe}(\text{TPP})_2\text{O}]$ <sup>32</sup> (2.087 Å),  $[\text{FeB}]_2\text{O}\cdot 2/3\text{DMF}$ <sup>33</sup> (2.04 Å),  $[\text{Fe}(\text{salen})]_2\text{O}\cdot 2\text{py}$ <sup>34</sup> (2.09 Å),  $[\text{Fe}(\text{salen})]_2\text{O}\cdot \text{CH}_2\text{Cl}_2$ <sup>35</sup> (2.11, <sup>35a</sup> 2.12<sup>35b</sup>

(28) Sinn, E.; Sim, G.; Dose, E. V.; Tweedle, M. F.; Wilson, L. J. *J. Am. Chem. Soc.* **1978**, *100*, 3375-3390.

(29) Oliver, J. D.; Mullica, D. F.; Hutchinson, B. B.; Milligan, W. D. *Inorg. Chem.* **1980**, *19*, 165-169.

(30) Lippard, S. J.; Schugar, H. J.; Walling, C. *Inorg. Chem.* **1967**, *6*, 1825-1831.

(31) Fleischer, E. B.; Hawkinson, S. *J. Am. Chem. Soc.* **1967**, *89*, 720-721.

(32) Hoffman, A. B.; Collins, D. M.; Day, V. W.; Fleischer, E. B.; Srivastava, T. S.; Hoard, J. L. *J. Am. Chem. Soc.* **1972**, *94*, 3620-3626.

(33) Gözen, S.; Peters, R.; Owston, P. G.; Tasker, P. A. *J. Chem. Soc., Chem. Commun.* **1980**, 1199-1201.

(34) Gerloch, M.; McKenzie, E. D.; Towl, A. D. C. *J. Chem. Soc. A.* **1969**, 2850-2858.

(35) (a) Coggon, P.; McPhail, A. T.; Mabbs, F. E.; McLachlan, V. N. *J. Chem. Soc. A.* **1971**, 1014-1019. (b) Atovmyan, L. O.; D'yachenko, O. A.; Soboleva, S. V. *Russ. J. Struct. Chem. (Engl. Transl.)* **1970**, *11*, 517-518.

Å), [Fe(sal-N-*n*-C<sub>3</sub>H<sub>7</sub>)<sub>2</sub>]<sub>2</sub>O<sup>36</sup> (2.14 Å), [Fe(2-mequin)<sub>2</sub>]<sub>2</sub>O·CHCl<sub>3</sub><sup>38</sup> (2.19 Å), [Fe(Cl-C<sub>7</sub>H<sub>2</sub>NO<sub>4</sub>)(H<sub>2</sub>O)<sub>2</sub>]<sub>2</sub>O·4H<sub>2</sub>O<sup>39</sup> (2.107 Å), and [Fe(C<sub>22</sub>H<sub>22</sub>N<sub>4</sub>)<sub>2</sub>]<sub>2</sub>O·CH<sub>3</sub>CN<sup>37</sup> (2.05 Å).

Another binuclear complex of interest for purposes of comparison is (C<sub>5</sub>H<sub>12</sub>N)<sub>3</sub>[(CH<sub>3</sub>COO){Fe(C<sub>6</sub>H<sub>4</sub>O<sub>2</sub>)<sub>2</sub>]<sub>2</sub>,<sup>9</sup> which contains two iron(III) atoms bridged by a single bidentate acetate moiety and by two oxygen atoms from separate catechol groups. The Fe–O(acetate) and Fe–O(bridge catecholate) distances in this complex (2.03 and 2.02 Å, respectively) are close to the mean Fe–O(carboxylate) lengths in **1** and **2** (2.048 Å), whereas the terminal Fe–O distances are somewhat shorter (1.97 Å). The structure of the basic iron carboxylates, [Fe<sub>3</sub>O(O<sub>2</sub>CR)<sub>6</sub>(H<sub>2</sub>O)<sub>3</sub>]<sup>+</sup>, consists of iron(III) atoms bridged by bidentate acetate groups with Fe–O(acetate) bond lengths typically in the range 1.96–2.08 Å; the mean distance in [Fe<sub>3</sub>O(gly<sup>+</sup>)<sub>6</sub>(H<sub>2</sub>O)<sub>3</sub>](ClO<sub>4</sub>)<sup>40</sup> is 2.02 Å, in [Fe<sub>3</sub>O(O<sub>2</sub>CCH<sub>3</sub>)<sub>6</sub>(H<sub>2</sub>O)<sub>3</sub>](ClO<sub>4</sub>)<sup>41</sup> it is 2.02 Å, and in [Fe<sub>3</sub>O(piv)<sub>6</sub>(MeOH)<sub>3</sub>]<sup>+</sup>Cl<sup>42</sup> it is 2.01 Å. A similarity in the overall structural features of the bridged cores of **1** and **2** and that of the Fe<sub>3</sub>O(O<sub>2</sub>CR)<sub>6</sub><sup>+</sup> complexes is expected since the unit consisting of any two iron atoms in the trinuclear cluster along with their bridging groups (i.e., Fe<sub>2</sub>(μ<sub>3</sub>-O)(μ-O<sub>2</sub>CR)<sub>2</sub>) has a distinct resemblance to the Fe<sub>2</sub>(μ-O)(μ-O<sub>2</sub>CCH<sub>3</sub>)<sub>2</sub> core in **1** and **2** (vide infra).

The Fe–O(oxo) distances in **1** and **2** (1.777 (3)–1.788 (2) Å) are equal and fall within the range 1.73 to 1.82 Å found for the single oxygen atom bridged binuclear iron(III) complexes mentioned above and for the structures of Fe<sub>2</sub>OCl<sub>6</sub><sup>2-</sup>.<sup>43</sup> Owing to the influence of the two acetate bridges the Fe–O–Fe angle (av. 124.6°) is well outside the range for the single-atom-bridged complexes (~139–180°) and is closer to the 120° Fe–O(oxo)–Fe angle found in the planar Fe<sub>3</sub>O<sup>7+</sup> unit.<sup>40,41</sup> The latter feature is responsible for an unusually short Fe···Fe distance (3.157 (1) Å) compared to other μ-oxo complexes (3.4–3.6 Å). The lengthened Fe···Fe separation (~3.3 Å) in the Fe<sub>3</sub>O<sup>7+</sup> core arises from the longer Fe–O(oxo) distances (1.9 Å). A lengthening in the Fe–N distances trans to the bridging oxo ligand indicates the greater structural trans effect<sup>44</sup> of oxo compared to carboxylato oxygen donor atoms and is also observed in the metmyohemerythrin crystal structure determination (vide infra). The geometry of the carboxylate ligands is unexceptional with mean angles and distances—O···O (**1**, 2.236 Å; **2**, 2.245 Å), C–O (**1**, 1.258 Å; **2**, 1.247 Å), O–C–O (**1**, 129°; **2**, 128.4°), C–C (**1**, 1.501 Å), C–C–O (**1**, 117.3°)—and the CH<sub>3</sub> (acetate) carbon atom lying in the plane of the carboxylate OCO group, in agreement with other carboxylate-bridged iron complexes.<sup>9,40,41</sup> The least-squares plane defined by the four non-hydrogen atoms in each acetate or the three non-hydrogen atoms in each formate group very nearly contains the two iron atoms (max deviation, 0.15 Å) indicating little "twist" of the carboxylate group relative to the iron–iron axis. By contrast, in another complex containing the M(μ-O)(μ-O<sub>2</sub>CCH<sub>3</sub>)<sub>2</sub>M core, Os<sub>2</sub>(μ-O)(μ-O<sub>2</sub>CCH<sub>3</sub>)<sub>2</sub>Cl<sub>4</sub>(PPh<sub>3</sub>)<sub>2</sub>(C<sub>2</sub>H<sub>5</sub>)<sub>2</sub>O,<sup>45</sup> the acetate groups are markedly twisted with respect to the Os–Os vector.

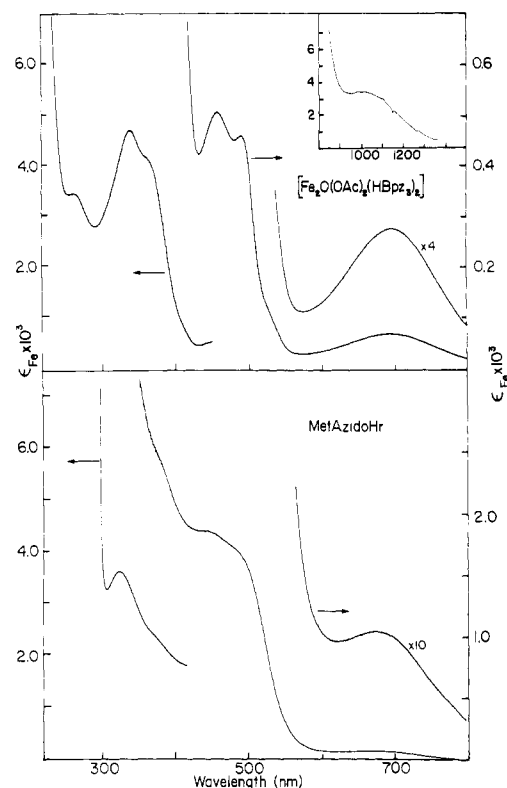


Figure 3. Optical spectra of **1** in CHCl<sub>3</sub> and metazidohemerythrin.

Finally, it should be noted that a complex containing the Fe<sub>2</sub>O(O<sub>2</sub>CCH<sub>3</sub>)<sub>2</sub><sup>2+</sup> core with a different capping tridentate amine has been structurally characterized.<sup>18</sup> In this complex, [Fe<sub>2</sub>O(O<sub>2</sub>CCH<sub>3</sub>)<sub>2</sub>(TCN)<sub>2</sub>]<sub>2</sub>I<sub>2</sub>·1/2NaI·3H<sub>2</sub>O, the structural parameters are very similar to those in **1** and **2** with some small differences. The [Fe<sub>2</sub>O(O<sub>2</sub>CCH<sub>3</sub>)<sub>2</sub>(TCN)<sub>2</sub>]<sup>2+</sup> cation exhibits typical Fe–O(oxo) (1.77 and 1.80 Å) and Fe–O(acetate) (2.00–2.05 Å) bond distances with a relatively short Fe···Fe separation (3.064 Å), consistent with a small Fe–O(oxo)–Fe angle (118.3°). The average Fe–N bond distance (2.18 Å) and lengthening in Fe–N bonds trans to the bridging oxo atom are also in close agreement with the appropriate values for **1** and **2**. A more detailed comparison must await report of the full structural details.

**Electronic Spectra.** The UV–vis–near IR spectrum of **1** in CHCl<sub>3</sub> solution is shown in Figure 3 together with that of azidomethemerythrin. The latter was recorded on a sample of the protein kindly provided by Dr. J. Sanders-Loehr.

Qualitatively, the spectrum of **1** bears a striking resemblance to that of azidomethemerythrin (Figure 3). Quantitatively, however, the prominent peaks between 400 and 500 nm are six times less intense than those observed in the spectrum of the protein sample.<sup>46</sup> The fact that **1**, **2**, **3**, and [Fe<sub>2</sub>O(O<sub>2</sub>CCH<sub>3</sub>)<sub>2</sub>(TCN)<sub>2</sub>]<sup>2+</sup><sup>18</sup> have nearly identical visible spectra indicates that this spectrum is characteristic of the {Fe<sub>2</sub>O(O<sub>2</sub>CR)<sub>2</sub>} core. The visible spectrum of the protein consists of the sum of these inherent optical transitions plus any applicable exogenous ligand-to-metal charge-transfer bands (e.g., azide to iron). As expected from this analysis, the spectra of methemerythrin and metchlorohemerythrin between 400 and 500 nm have peaks with intensities similar to those in the spectra of **1**–**3**.

Although we do not yet have enough information to assign completely the electronic spectra of **1**, **2**, and **3**, several comments can be made. The high-spin, oxo-bridged diiron(III) complex, [Fe<sub>2</sub>O(HBpz<sub>3</sub>)<sub>2</sub>(H<sub>2</sub>Bpz<sub>2</sub>)<sub>2</sub>], containing poly(pyrazolylborate) ligands but lacking the bridging acetate ligands fails to show any

(36) Davies, J. E.; Gatehouse, B. M. *Cryst. Struct. Commun.* **1972**, *1*, 115–120.

(37) Weiss, M. C.; Goedken, V. L. *Inorg. Chem.* **1979**, *18*, 819–826.

(38) Mabbs, F. E.; McLachlan, V. N.; McFadden, D.; McPhail, A. T. *J. Chem. Soc., Dalton Trans.* **1973**, 2016–2021.

(39) Ou, C. C.; Wollman, R. G.; Hendrickson, D. N.; Potenza, J. A.; Schugar, H. J. *J. Am. Chem. Soc.* **1978**, *100*, 4717–4724.

(40) Thundathil, R. V.; Holt, E. M.; Holt, S. L.; Watson, K. J. *J. Am. Chem. Soc.* **1977**, *99*, 1818–1823.

(41) Anzenhofer, K.; DeBoer, J. *Recl. Trav. Chim., Pays-Bas* **1969**, *88*, 286–288.

(42) Blake, A. B.; Fraser, L. R. *J. Chem. Soc., Dalton Trans.* **1975**, 193–197.

(43) (a) Drew, M. G. B.; McKee, V.; Nelson, S. M. *J. Chem. Soc., Dalton Trans.* **1978**, 80–84. (b) Schmidbaur, H.; Zybilla, C. E.; Neugebauer, D. *Angew. Chem., Int. Ed. Engl.* **1983**, *22*, 156 and 161. (c) Dehnicke, K.; Prinz, H.; Massa, W.; Pebler, J.; Schmidt, R. *Z. Anorg. Allg. Chem.* **1983**, *499*, 20–30. (d) Reiff, W. M.; Brennan, T. F.; Garofalo, A. R. *Inorg. Chim. Acta* **1983**, *77*, L83–L88.

(44) Appleton, T. G.; Clark, H. C.; Manzer, L. E. *Coord. Chem. Rev.* **1973**, *10*, 335–422.

(45) Armstrong, J. E.; Robinson, W. R.; Walton, R. A. *Inorg. Chem.* **1983**, *22*, 1301–1306.

(46) (a) Sanders-Loehr, J.; Loehr, T. M.; Mauk, A. G.; Gray, H. B. *J. Am. Chem. Soc.* **1980**, *102*, 6992–6996. (b) Dunn, J. B. R.; Addison, A. W.; Bruce, R. E.; Sanders-Loehr, J.; Loehr, T. M. *Biochemistry* **1977**, *8*, 1743–1749. (c) Garbett, K.; Darnall, D. W.; Klotz, I. M.; Williams, R. J. *P. Arch. Biochem. Biophys.* **1969**, *103*, 419–434.

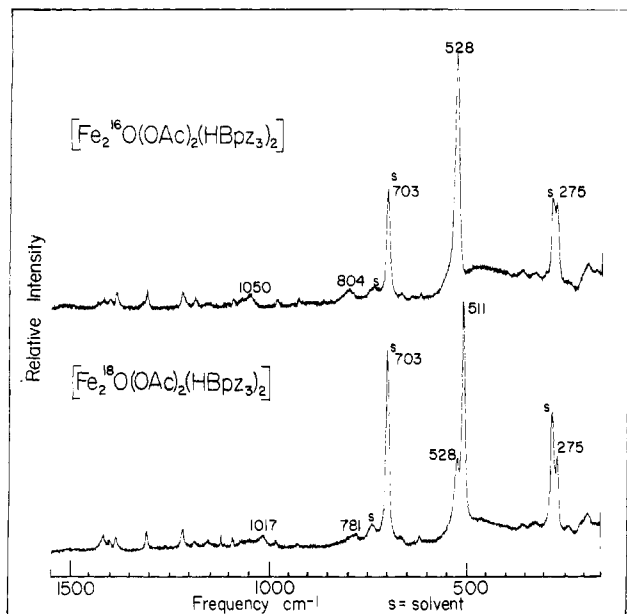


**Figure 4.** Resonance Raman spectra of **1** and its  $^{18}\text{O}$ -substituted derivative in  $\text{CH}_2\text{Cl}_2$  solution.

peaks in its visible spectrum above 400 nm.<sup>47</sup> This observation, coupled with the similarity between the visible spectra of **1–3** and  $[\text{Fe}_2\text{O}(\text{O}_2\text{CCH}_3)_2(\text{TCN})_2]^{2+}$ , rules out the possibility that ligand-to-metal charge transfer involving the pyrazolylborate ligands is responsible for any of the visible bands, especially the more prominent ones at 457 ( $\epsilon_{\text{max}} 505 \text{ cm}^{-1} \text{ M}_{\text{Fe}}^{-1}$ ) and 492 nm ( $\epsilon_{\text{max}} 460 \text{ cm}^{-1} \text{ M}_{\text{Fe}}^{-1}$ ). Moreover, these bands are too intense for d-d transitions, even those enhanced by lowered symmetry or spin-spin interactions between the metal ions. Since neither of these bands is responsible for the resonance Raman enhancement of  $\nu_s(\text{Fe}-\text{O}-\text{Fe})$  in the visible region (vide infra), they are unlikely to involve charge-transfer transitions arising from the  $\mu$ -oxo bridge.

Four d-d transitions are expected for octahedral high-spin  $d^5$  ferric complexes.<sup>48</sup> The two lowest in energy,  ${}^6\text{A}_1 \rightarrow {}^4\text{T}_2({}^4\text{G})$  and  ${}^5\text{A}_1 \rightarrow {}^4\text{T}_1({}^4\text{G})$ , are readily observed at 695 ( $\epsilon_{\text{max}} 70 \text{ cm}^{-1} \text{ M}_{\text{Fe}}^{-1}$ ) and 995 nm ( $\epsilon_{\text{max}} 3.5 \text{ cm}^{-1} \text{ M}_{\text{Fe}}^{-1}$ ), respectively. Both here and in the methemerythrins, the other two transitions are "buried" under the more intense visible transitions.<sup>46a</sup> These d-d transitions, especially if they contain some charge-transfer character, may in fact be just those hidden bands responsible for the  $\sim 10$ -fold (weak) resonance enhancement of the Raman spectrum in the visible region (vide infra). This assignment would place the  ${}^6\text{A}_1 \rightarrow [{}^4\text{A}_1, {}^4\text{E}]({}^4\text{G})$  transition at  $\sim 520 \text{ nm}$  and the  ${}^6\text{A}_1 \rightarrow {}^4\text{T}_2({}^4\text{D})$  transition at  $\sim 440 \text{ nm}$  (if **1–3** are indeed analogous to the azidomethemerythrin).<sup>49</sup>

**Resonance Raman and Fourier Transform Infrared Spectroscopy.** The resonance Raman spectrum of a 0.1 M solution of **1** in methylene chloride is shown in Figure 4, top. In order definitively to identify those lines which represent vibrations of the ( $\mu$ -oxo)diiron(III) unit, the spectrum of  $^{18}\text{O}$ -exchanged **1** was recorded and is shown in Figure 4, bottom. Four features clearly shifted upon isotopic substitution. We assign the line at  $528 \text{ cm}^{-1}$  to the symmetrical Fe-O-Fe stretch ( $\nu_s$ ) and note that  $^{18}\text{O}$  exchange shifts it to  $511 \text{ cm}^{-1}$ . The feature at  $1050 \text{ cm}^{-1}$  appears to contain more than one line, only one of which shifts (to  $1017 \text{ cm}^{-1}$ ) in the  $^{18}\text{O}$  spectrum. Since  $1050 \text{ cm}^{-1} \approx 2 \nu_s$ , we assign this shiftable line to the first overtone of the symmetric stretch. Although changes clearly occur in the region around  $280 \text{ cm}^{-1}$  upon  $^{18}\text{O}$  substitution, it is uncertain exactly what shift is taking place owing to the presence of a strong solvent band at  $285 \text{ cm}^{-1}$ . Since other good solvents for **1** also have peaks in this region,

#### FOURIER TRANSFORM INFRARED SPECTRA OF $[\text{Fe}_2\text{O}(\text{OAc})_2(\text{HBpz}_3)_2]$

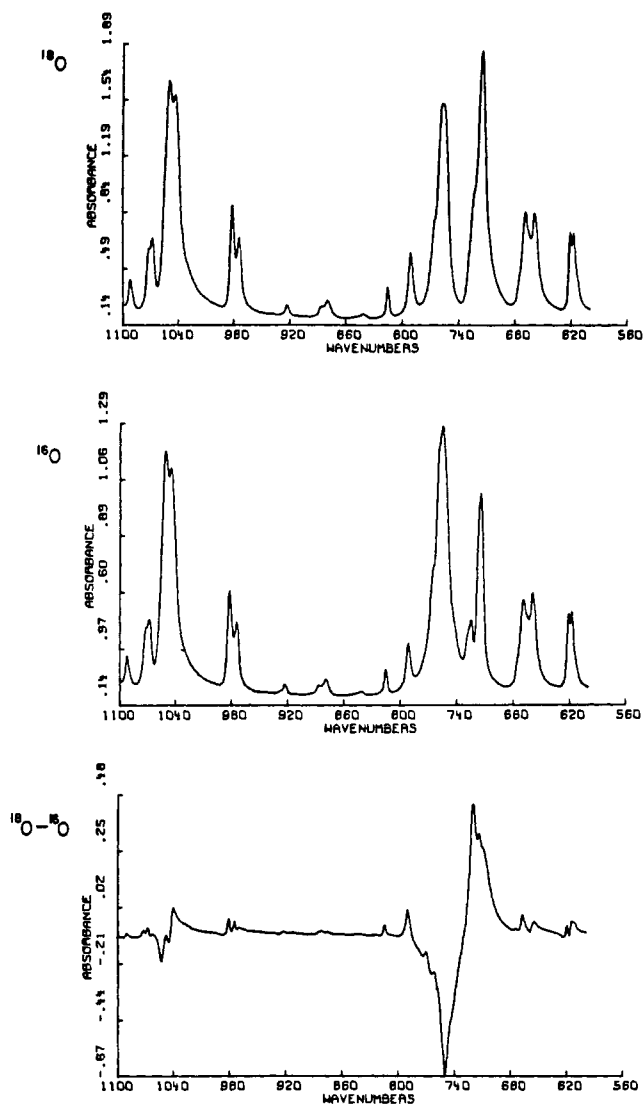


**Figure 5.** Fourier transform infrared spectra of  $^{18}\text{O}$ -**1**,  $^{16}\text{O}$ -**1**, and the difference between these spectra. Samples were run in KBr for 32 scans at  $2\text{-cm}^{-1}$  resolution.

spectra were taken of solid samples of **1** and its  $^{18}\text{O}$ -substituted analogue. These spectra show a line at  $269 \text{ cm}^{-1}$  which does not shift upon  $^{18}\text{O}$  substitution and a broad feature at  $278 \text{ cm}^{-1}$  which moves under the  $269\text{-cm}^{-1}$  line after  $^{18}\text{O}$  exchange. Closer examination of the solution spectra in Figure 4, top, reveals the presence of a shoulder around  $300 \text{ cm}^{-1}$  which shifts under the solvent line, increasing its intensity in the  $^{18}\text{O}$  spectrum, Figure 4, bottom. We assign the feature at  $278 \text{ cm}^{-1}$  in the solid state (and at an undetermined position in solution) to the deformation mode of the Fe-O-Fe unit,  $\nu_d$ . Finally, a broad feature at  $804 \text{ cm}^{-1}$  shifts to  $781 \text{ cm}^{-1}$  after  $^{18}\text{O}$  exchange, leaving behind a line at  $791 \text{ cm}^{-1}$ . It is possible that this shiftable line is the asymmetric Fe-O-Fe stretch since this vibration is Raman allowed in  $C_{2v}$  symmetry and would be expected to occur in this region.<sup>8b,43a,50,51</sup> Investigators studying azidomethemerythrin have assigned a band at  $780 \text{ cm}^{-1}$  to this asymmetric stretch for just these reasons.<sup>49</sup> We are unable to make such an assignment, however, because the infrared spectrum shows only one band of very weak intensity in this region which does not move at all with  $^{18}\text{O}$  substitution.

(47) Armstrong, W. H.; Lippard, S. J., unpublished results.

(48) Hush, N. S.; Hobbs, R. J. M. *Prog. Inorg. Chem.* **1968**, *10*, 259–359.

(49) Shienme, A. K.; Loehr, T. M.; Sanders-Loehr, J., submitted for publication.

(50) Khedekar, A. V.; Lewis, J.; Mabbs, F. E.; Weighold, H. J. *Chem. Soc. A* **1967**, 1561–1564.

(51) Solbrig, R. M.; Duff, L. L.; Shriver, D. F.; Klotz, I. M. *J. Inorg. Biochem.* **1982**, *17*, 69–74.

The 804-cm<sup>-1</sup> feature must therefore be accounted for in some other way. The presence of a line at 791 cm<sup>-1</sup> may obscure the true maximum position of this line. We note that  $\nu_s + \nu_d = 808$  cm<sup>-1</sup>, and therefore tentatively assign the line at 804 cm<sup>-1</sup> to the combination band  $\nu_s + \nu_d$ .

In order to obtain further information about the asymmetric Fe-O-Fe stretching vibrations, commonly used to identify ( $\mu$ -oxo)diiron(III) complexes,<sup>8b,43a,50,51</sup> Fourier transform infrared spectra of solid samples of **1** and <sup>18</sup>O-**1** were recorded from 600 to 1100 cm<sup>-1</sup>. These spectra and the <sup>18</sup>O - <sup>16</sup>O difference spectrum are displayed in Figure 5. From these spectra it is evident that the  $\nu_{as}$ (Fe-O-Fe) mode shifts from 751 (<sup>16</sup>O) to 721 cm<sup>-1</sup> (<sup>18</sup>O) upon isotopic substitution, from under one ligand band to under another. Its surprisingly low intensity and energy require comment. Both are probably the result of the small Fe-O-Fe angle. Walton et al. were unable to find an asymmetric  $\mu$ -oxo stretch in the infrared spectrum of an analogous osmium complex,<sup>45</sup> and in Fe<sub>2</sub>O(phen)<sub>2</sub>(SO<sub>4</sub>)<sub>2</sub>·6H<sub>2</sub>O, where one of the sulfate groups bridges the iron atoms along with the  $\mu$ -oxo ligand, the asymmetric vibration is also surprisingly weak.<sup>10</sup> These compounds also have unusually acute M-O-M angles. No asymmetric stretches have been identified for the [Fe(salen)]<sub>2</sub>O complexes either.<sup>8b</sup> These complexes had the smallest reported Fe-O-Fe angles, except for the hemerythrin, prior to our communication of the structure of **1**.<sup>15</sup> The change in the dipole moment diminishes for this vibrational mode when the M-O-M angle decreases reducing the intensity of the infrared asymmetric stretching band. In the [Fe<sub>2</sub>O(O<sub>2</sub>CCH<sub>3</sub>)<sub>2</sub>(TCN)<sub>2</sub>]<sup>2+</sup> cation, where the Fe-O-Fe angle is even smaller,  $\nu_{as}$ (Fe-O-Fe) occurs at 730 cm<sup>-1</sup>.<sup>18</sup> This observation is consistent with the above arguments.

A simplified set of secular equations (eq 1 and 2, where  $\mu_M$  and  $\mu_O$  are reciprocals of the masses of metal and oxygen, respectively,  $\lambda_i = (5.889 \times 10^{-7})\nu_i^2$  where  $\nu_i$  is the frequency of the *i*th vibration in wave numbers,  $k_d$  is the M-O stretching force constant in mdyn/Å, and  $k_{dd}$  is the M-O-M stretch-stretch interaction force constant in mdyn/Å), previously derived<sup>52</sup> for singly bridged bimetallic coordination compounds of C<sub>2v</sub> symmetry, may be applied to the vibrational analysis of **1**. From measured values

$$A_1 \quad \lambda_s = [\mu_M + \mu_O(1 + \cos \phi)](k_d + k_{dd}) \quad (1)$$

$$B_1 \quad \lambda_{as} = [\mu_M + \mu_O(1 - \cos \phi)](k_d - k_{dd}) \quad (2)$$

of  $\nu_s$  and  $\nu_{as}$  the stretch ( $k_d$ ) and the stretch-stretch interaction ( $k_{dd}$ ) force constants are easily calculated to be  $k_d = 3.24$  mdyn/Å and  $k_{dd} = 0.35$  mdyn/Å. From these constants, the  $\nu_s$  and  $\nu_{as}$  values for the <sup>18</sup>O substituted derivative of **1** may also be computed. The results are  $\nu_s = 510$  cm<sup>-1</sup>, which is identical within experimental error with the measured value of 511 cm<sup>-1</sup>, and  $\nu_{as} = 715$  cm<sup>-1</sup>, which is somewhat less than the observed value (721 cm<sup>-1</sup>). Possibly the numbers obtained from the FTIR difference spectrum are not as accurate as we might wish, although a difference of 6 cm<sup>-1</sup> between observed and calculated values is not substantial. It is interesting that the stretching force constant ( $k_d$ ) for **1** is identical with the one calculated for Fe<sub>2</sub>OCl<sub>6</sub><sup>2-</sup>.<sup>51</sup>

Many of the remaining Raman bands in **1**, **2**, and **3** also occur in [Fe(HBpz<sub>3</sub>)<sub>2</sub>]<sup>+</sup> and are assigned to the vibrations of the pyrazolylborate ligand. These bands as well as those assigned previously are summarized in Table V. A Raman spectrum of NaHBpz<sub>3</sub> exhibits bands that may correspond to those in the iron complexes, but these were often as much as 30 cm<sup>-1</sup> from the corresponding bands of the coordinated ligand.

Of the remaining lines observed in the Raman spectrum of **1**, three (275, 328, and 360 cm<sup>-1</sup>) are absent in the spectra of Fe-(HBpz<sub>3</sub>)<sub>2</sub><sup>+</sup> but occur (within  $\pm 10$  cm<sup>-1</sup>) in the spectra of the formate- (**2**) and benzoate-bridged (**3**) analogues. The line at 269 cm<sup>-1</sup> in the solid spectrum of **1** and at 275 cm<sup>-1</sup> in solution is in the right frequency range for an Fe-N stretch<sup>10b,53</sup> and so we tentatively make this assignment. Since the structures of **1-3** are all very similar it is reasonable to expect the symmetric Fe-O-

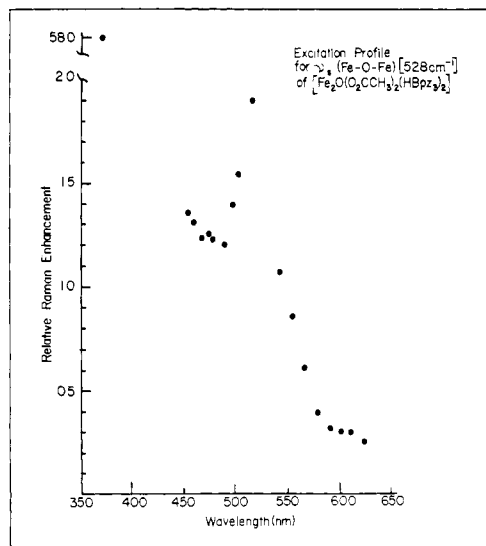


Figure 6. Excitation profile of the 528-cm<sup>-1</sup> ( $\nu_s$ , Fe-O-Fe) Raman band of **1**.

(carboxylate) stretching frequency to occur at nearly the same frequency in the three complexes, i.e., either at 328 or 360 cm<sup>-1</sup>. Since the line at 360 cm<sup>-1</sup> is more intense in the spectra of the three complexes and closer in frequency to where such an Fe-O carboxylate stretch might be expected,<sup>53</sup> we tentatively assign the band to the symmetrical Fe-O(carboxylate) stretching mode. The remaining lines in the spectra of **1-3** are presently unassignable.

To aid in the analysis of the vibrational spectra, **1** was synthesized by using <sup>18</sup>OH<sub>2</sub> (99% enriched, diluted 1:2 with <sup>16</sup>OH<sub>2</sub>) in the expectation of incorporating <sup>18</sup>O into the bridging position. The 3:2 ratio of peaks at 511 and 528 cm<sup>-1</sup> in the resonance Raman spectrum of this <sup>18</sup>O-substituted derivative in methylene chloride (~0.1 M) indicated that there was 60% incorporation of <sup>18</sup>O into the Fe-O-Fe unit. At a later time, however, the same solution gave a spectrum in which the 511-cm<sup>-1</sup> band was less than 10% of  $\nu_s$ (Fe-O-Fe). This result not only demonstrated that water from air readily exchanges its oxygen with the bridging oxygen atom of **1** in methylene chloride but it also suggested a simple method for preparing <sup>18</sup>O-substituted **1**. A solution of **1** in methylene chloride in a sealed vial was stirred with <sup>18</sup>O (99%—only small quantities are needed). The solid-state Raman spectra of **1** prepared this way showed essentially 100% <sup>18</sup>O substitution at the oxo position. Mass spectra of these samples show 85% incorporation of <sup>18</sup>O due to handling of solutions of **1** in air with the resultant <sup>16</sup>O exchange and, more importantly, demonstrate that only the bridging oxygen exchanges. In the protein, exchange only occurs under certain conditions and in particular metazidohemerythrin in <sup>18</sup>OH<sub>2</sub> will not exchange at all.<sup>49,68</sup> The rapid exchange (see above) of <sup>18</sup>O for <sup>16</sup>O in the bridge position of our model compound suggests that the lack of exchange in the protein is caused by inaccessibility of water to the diiron core and is not an intrinsic property of the [Fe<sub>2</sub>O(O<sub>2</sub>CR)<sub>2</sub>] active site.

The excitation profile for the 528-cm<sup>-1</sup> ( $\nu_s$ ) band of **1** is shown in Figure 6. It is remarkably similar to the excitation profile of the 503-cm<sup>-1</sup> ( $\nu_s$ ) line of azidomethemerythrin.<sup>46b,49</sup> The profile in Figure 6 peaks at ~520 nm, near the region where the profile peak of the protein band occurs. This value is significantly lower in energy than the major peak at 492 nm in the optical spectrum, but close to a weak shoulder (528 nm). The profile of the symmetric stretch in the azidomethemerythrin also has a peak at around 440 nm.<sup>49</sup> In the profile of the symmetric stretch of **1**, the band intensity is observed to be rising at 454 nm as the excitation wavelength decreases, but precisely where it reaches a maximum cannot be determined with the data at hand. We

(52) (a) Wing, R. M.; Callahan, K. P. *Inorg. Chem.* **1969**, *4*, 871-874. (b) Cotton, F. A.; Wing, R. M. *Inorg. Chem.* **1965**, *6*, 867-873.

(53) Ferraro, J. R. "Low-Frequency Vibrations of Inorganic and Coordination Compounds"; Plenum Press: New York, 1971; see, for example, p 201 and also Chapter 5.

Table V. Observed Raman Lines and Their Proposed Assignments<sup>a</sup>

[Fe <sub>2</sub> O(O <sub>2</sub> CCH <sub>3</sub> ) <sub>2</sub> (HBpz <sub>3</sub> ) <sub>2</sub> ] (1)	[Fe <sub>2</sub> O(O <sub>2</sub> CH) <sub>2</sub> (HBpz <sub>3</sub> ) <sub>2</sub> ] (2)	[Fe <sub>2</sub> O(O <sub>2</sub> CPh) <sub>2</sub> (HBpz <sub>3</sub> ) <sub>2</sub> ] (3)	[Fe(HBpz <sub>3</sub> ) <sub>2</sub> ]ClO <sub>4</sub>	assignment <sup>b</sup>
	185			
173		164	169	
	185		199	
193				
208 sh	215	212 sh		
		229		
248		244		
274 s	278 s	(under solvent 285)		$\nu_s(\text{Fe-N})$
283	285	285	285	solvent
			300	$\nu_s(\text{Fe-N})$
301 sh				$\delta(\text{Fe-O-Fe})$
328	334 sh	337		
	339 sh			
360	359	360		$\nu_s(\text{Fe-O}_2\text{CR})$
528 s <sup>c</sup>	525 s	526 s		$\nu_s(\text{Fe-O-Fe})$
			556 b	
621		621 w		
669	668	667	674	L
703	703	703	703	solvent
740 b	740 b	740 b	729 b	solvent
791			798	L
804	802	812		L
808 <sup>c</sup>				$\nu_s + \nu_d^d$
865 w	837 sh	839	865 w	
	884 w		920 m	
929	927	929	927	L
981	983	981	993	L
1050			1049	L
1050 <sup>c</sup>	1046	1062 b		$2\nu_s^e$
1070	1068		1075	L
1092	1087	1094	1109	L
			1119	$\nu_3(\text{ClO}_4^-)$
1156 b	1157	1155		solvent
1188	1187	1190	1189	L
1220	1220	1217	1213	L
			1224 sh	
1310	1310	1312	1314	L
1321 sh	1321 sh		1320	L
1387	1389	1392	1388	L
1403	1404	1405	1408	solvent
1436	1434 sh	1433 sh	1446 w	L
		1493		

<sup>a</sup> Entries are in cm<sup>-1</sup>. Symbols: s, strong; w, weak; sh, shoulder; b, broad. The table covers only the range 160–1500 cm<sup>-1</sup>. All compounds were dissolved in CH<sub>2</sub>Cl<sub>2</sub>. <sup>b</sup>  $\nu_s$  = symmetric stretch,  $\delta$  = deformation, L = assigned as vibration of HBpz<sub>3</sub><sup>-</sup>. <sup>c</sup> Shifts upon exchange with <sup>18</sup>O<sub>2</sub> (see text). <sup>d</sup> Combination band. <sup>e</sup> Overtone.

suspect that it also reaches a maximum at  $\sim 440$  nm before it rises to  $\sim 100$ -fold enhancement at 364 nm (Figure 6).

Qualitatively, the 1050- and 804-cm<sup>-1</sup> lines follow the same enhancement profile as the 528-cm<sup>-1</sup> band (data not shown) as expected, but the low relative intensities of these lines and the fact that both overlap other lines make it difficult to determine their profiles quantitatively.

**Mössbauer Spectra.** The Mössbauer spectra at 4.2 and 170 K consist of a symmetric quadrupole doublet. The 4.2 K spectrum is shown in Figure 7a. A least-squares fit (solid line) to the experimental points assuming Lorentzian absorption lines gives an isomer shift  $\delta = 0.52 \pm 0.03$  mm/s (relative to metallic iron at room temperature) and a quadrupole splitting  $\Delta E_Q = 1.60 \pm 0.05$  mm/s. The observed line widths (full width at half maximum  $\Gamma = 0.31 \pm 0.04$  mm/s) are consistent with equivalent iron sites. Since the isomer shifts for a large number of high-spin mononuclear and  $\mu$ -oxo-bridged binuclear ferric complexes generally fall in the range 0.3 to 0.6 mm/s,<sup>54</sup> the isomer shift for **1** is indicative of a high-spin ferric state. The quadrupole splitting for **1**, however, is substantially larger than for most  $S = 5/2$  ferric complexes. On the other hand, several  $\mu$ -oxo-bridged complexes<sup>5b</sup>

and the met forms of hemerythrin<sup>26,55</sup> have  $|\Delta E_Q|$  values in the range 1.5–2.0 mm/s, which encompasses the parameters derived for **1**.

The Mössbauer spectra of **1** in externally applied magnetic fields,  $H_0 \leq 80$  kOe at 4.2 K, are consistent with those of a diamagnetic ground state. The experimental spectrum obtained at  $H_0 = 40$  kOe is shown in Figure 7c. A characteristic doublet-triplet absorption pattern occurs that is characteristic of a negative sign for the principal component of the electric field gradient ( $V_{zz}$ ).<sup>55</sup> The negative sign of  $V_{zz}$  indicates a distortion from octahedral symmetry which corresponds to a compression along a symmetry axis. For all but one of the met forms of hemerythrin the sign of  $V_{zz}$  has been determined to be positive. A theoretical simulation of the data in Figure 7c, assuming random orientation of the crystallites in the powdered sample relative to the direction of  $H_0$ , is given in Figure 7b. The simulation parameters were the field at the nucleus  $H_n = 40$  kOe,  $\Delta E_Q = -1.60$  mm/s,  $\Gamma = 0.31$  mm/s, and the asymmetry parameter  $\eta = 0$ . Simulations for  $H_0 = 20, 60,$  and  $80$  kOe were also carried out and fit the experimental data very well with  $H_n = H_0$  in all cases. In other words, there is no detectable contribution from magnetic hyperfine interaction other

(54) Greenwood, N. N.; Gibb, T. C. "Mössbauer Spectroscopy"; Chapman and Hall, Ltd.: London, 1971; pp 148–164.

(55) (a) Collins, R. L. *J. Chem. Phys.* **1965**, *42*, 1072–1080. (b) Gabriel, J. R.; Ruby, S. L. *Nucl. Instrum. Methods* **1965**, *36*, 23–28.

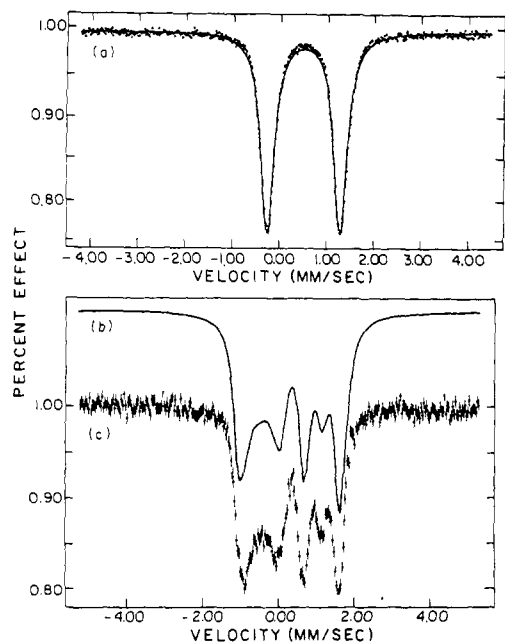


Figure 7. (a) Mössbauer spectrum of **1** in zero applied field at 4.2 K. (b) Simulation of  $H_0 = 40$  kOe Mössbauer spectrum of **1**. The experimental spectrum is given in c.

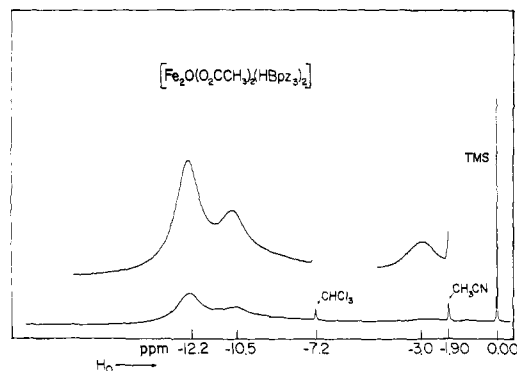


Figure 8. Proton NMR spectrum of **1** in  $\text{CDCl}_3$ .

than the applied field and therefore no residual paramagnetism at 4.2 K.

**NMR Spectra.** Proton NMR spectroscopy has proved to be a very useful technique for monitoring reaction products in this study. Distinguishing between the low-spin monomeric ferric species and the coupled high-spin species is quite straightforward. Compounds **1**–**3** were examined over the range  $\pm 200$  ppm.

The  $^1\text{H}$  NMR spectrum of **1** in  $\text{CDCl}_3$  solution at 295 K is shown in Figure 8. Superficially, the spectrum appears to consist of three broad resonances at  $-12.3$ ,  $-10.5$ , and  $-3.0$  ppm. There is evidence, however, for an even broader resonance underlying the  $-10.5$ -ppm peak. Examination of the spectra of  $[\text{Fe}_2\text{O}(\text{O}_2\text{CH})_2(\text{HBpz}_3)_2]$  and  $[\text{Fe}_2\text{O}(\text{O}_2\text{CCD}_3)_2(\text{HBpz}_3)_2]$ , in which the  $-10.5$  ppm resonance is absent, revealed an underlying signal at ca.  $-9.1$  ppm. From this result we assign the  $-10.5$ -ppm resonance in **1** to the acetate methyl protons. The spectrum of  $[\text{Fe}_2\text{O}(\text{O}_2\text{CCH}_3)_2(\text{DBpz}_3)_2]$  lacks the signal at  $-3.0$  ppm, implying that this peak arises from H(B) in **1**.

From the  $C_{2v}$  symmetry found for **1** in the solid state, which should be retained in solution, one expects to find eight  $^1\text{H}$  resonances, including two sets of nonequivalent pyrazole ring resonances. Only four peaks are resolved, however, and we therefore assume that the  $^1\text{H}$  NMR signals of all the pyrazole rings are equivalent. Since the  $-12.3$ -ppm resonance is substantially more intense than any other, it is assigned to two accidentally degenerate proton resonances, tentatively, protons H(4) and H(5) of the pyrazole rings (atom labels are given in Table IV). The very broad signal at ca.  $-9.1$  ppm underlying the  $\text{CH}_3$  resonance is assigned

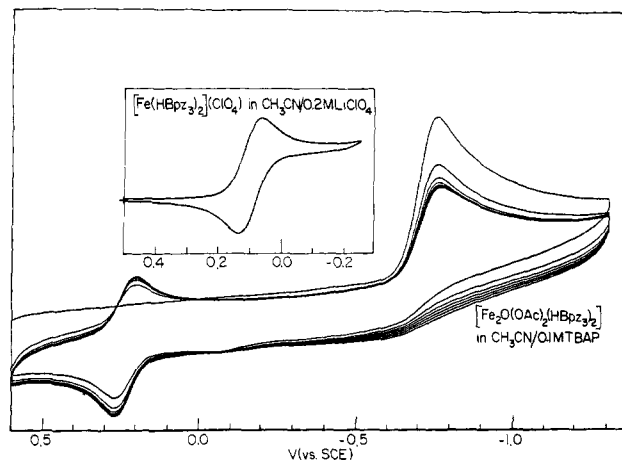


Figure 9. Cyclic voltammograms at  $200 \text{ mV s}^{-1}$  at a glassy carbon electrode of **1** in 0.1 M tetra-*n*-butylammonium perchlorate in acetonitrile showing several repetitive scans. The inset shows results for  $[\text{Fe}(\text{HBpz}_3)_2]^{n+}$ ,  $n = 0$  and 1, in 0.2 M  $\text{LiClO}_4/\text{CH}_3\text{CN}$  solution. Voltage readings are referenced to the saturated calomel electrode.

to H(3) of the pyrazole ring because it is the proton closest to the paramagnetic iron centers. It would be the broadest signal if the dipolar interaction were primarily responsible for the line broadening. In the simplest analysis, complex **1** may be considered as two separate  $S = 5/2$  iron(III) systems, in which the dipolar contribution to the isotropic shifts ( $\Delta H/H_0$ ) is usually negligible.<sup>56,57</sup> The observed isotropic shifts, then, are contact in origin. Shifts of the pyrazole ring protons are not attenuated by distance (assuming that the previous assignments hold) as would be expected if the shift mechanism were purely  $\sigma$  contact in nature. The pyrazole ring protons all have negative isotropic shifts compared to the potassium salt of the free ligand in  $\text{CDCl}_3$ . A purely  $\pi$ -spin delocalization mechanism is therefore also unlikely since contact shifted systems in which a  $\pi$  mechanism dominates exhibit an alternating sign pattern of shifts. The  $^1\text{H}$  NMR spectrum of the  $\mu$ -oxo-bridged complex,  $[\text{Fe}(\text{sal-}N\text{-}n\text{-C}_3\text{H}_7)_2]\text{O}$ , displays an alternating sign pattern around the aromatic ring, indicative of the  $\pi$ -spin delocalization mechanism.<sup>58</sup> An independent study on salen ( $\mu$ -oxo)diiron complexes confirmed this result.<sup>59</sup> In contrast, phenanthroline and bipyridine  $\mu$ -oxo-bridged complexes, e.g.,  $[\text{Fe}_2\text{O}(\text{phen})_4]\text{Cl}_4 \cdot 5\text{H}_2\text{O}$ <sup>57</sup> and  $[\text{Fe}_2\text{O}(\text{bpy})_4]\text{Cl}_4 \cdot 6\text{H}_2\text{O}$ ,<sup>60</sup> have spectra interpreted in terms of a predominantly  $\sigma$ -spin delocalization mechanism. The contact shifts in these complexes are generally larger than those in **1** and are all negative, except for small positive shifts for the H(4,7) in the phenanthroline complex and H(4,4') in the bipyridine complex. As in **1**, line widths for the proton closest to the paramagnetic center, H(6,6') in bpy and H(2,9) in phen, are substantially larger than the others.

Further studies, including temperature dependence and ring methyl substitutions, would be required to elucidate the relative contributions of  $\sigma$ - and  $\pi$ -spin delocalization mechanisms in **1**. NMR studies of azidomethemerythrin from *P. gouldii* at 250 MHz did not reveal either the histidine imidazole ring or the  $\beta$ - $\text{CH}_2$  protons of aspartate or the  $\gamma$ - $\text{CH}_2$  resonance of glutamate.<sup>61</sup> This result is somewhat surprising in light of the present work.

**Electrochemistry.** Figure 9 displays the cyclic voltammetry (CV) results for **1** in acetonitrile with 0.1 M TBAP as the supporting electrolyte. During the first cathodic sweep a reduction can be seen at  $-0.76$  V vs. SCE for which there is no coupled oxidation wave. Even at scan speeds of 5 V/s, little if any of the

(56) McGarvey, B. R.; Kurland, R. J. *J. Magn. Reson.* **1970**, *2*, 286–301.

(57) Wicholas, M. *J. Am. Chem. Soc.* **1970**, *92*, 4141–4142.

(58) Boyd, P. D. W.; Murray, K. S. *J. Chem. Soc. A.* **1971**, 2711–2714.

(59) LaMar, G. N.; Eaton, G. R.; Holm, R. H.; Walker, F. A. *J. Am. Chem. Soc.* **1973**, *95*, 63–75.

(60) Wicholas, M.; Jayne, D. *Inorg. Nucl. Chem. Lett.* **1971**, *7*, 443–445.

(61) York, J. L.; Millett, F. S.; Minor, L. B. *Biochemistry* **1980**, *19*, 2583–2588.

reduced form survives to be reoxidized. A small wave and an inflection can be seen in the return scan at  $-0.04$  and  $+0.11$  V, respectively, followed by a major oxidation wave at  $+0.26$  V. Continuous scans (Figure 9) reveal the formation of a stable new species with oxidation and reduction peak potentials at  $+0.26$  and  $+0.20$  V, respectively, and  $E_{1/2} = +0.23$  V. This value is exactly the half-wave potential of the  $[\text{Fe}(\text{HBpz}_3)_2]^+$  cation<sup>17</sup> measured under these conditions.

The inset to Figure 9 shows the CV results for  $[\text{Fe}(\text{HBpz}_3)_2]\text{ClO}_4$  over the range  $0.5$  to  $-0.2$  V. Here, in  $0.2$  M  $\text{LiClO}_4/\text{CH}_3\text{CN}$  solution, this Fe(II)/Fe(III) couple approaches electrochemical reversibility ( $\Delta E_p = 62$  mV).<sup>62</sup> The cathodic and anodic waves have equal heights ( $i_c = i_a$ ) and are superimposable. Similarly, symmetric CV's were recorded in dimethylformamide and methanol with  $0.1$  M TBAP and  $0.1$  M tetrabutylammonium acetate (TBAA) as supporting electrolytes. Finally, a plot of  $i_a$  or  $i_c$  vs.  $(v)^{1/2}$  ( $v$  = scan speed) is linear, further supporting the claim of reversibility in this system. A recent report of the electrochemistry of  $\text{Fe}(\text{HBpz}_3)_2$  shows that this couple is also reversible in liquid  $\text{SO}_2$ .<sup>63</sup>

In a separate experiment,  $[\text{Fe}(\text{HBpz}_3)_2]\text{ClO}_4$  was added to the cell containing **1**. The CV resembled that of Figure 9 except that the reversible wave at  $E_{1/2} = 0.23$  V grew proportionately in intensity. We therefore conclude that, upon reduction, **1** collapses irreversibly to mononuclear  $[\text{Fe}(\text{HBpz}_3)_2]$  and other, as yet unidentified, electrochemically inactive iron species.

The repetitive scans in Figure 9 show that there are no reduction waves corresponding to the features at  $-0.04$  and  $+0.11$  V in the anodic scan. Also, if the scan rate is slowed to  $20$  mV/s, these anodic waves are no longer evident. Intermediates in the decomposition of **1** are probably responsible for these features in the CV since they would be expected to be more evident at faster scan speeds, as is the case.

If the system is allowed to scan continuously for several cycles (Figure 9) a steady state is obtained at the electrode surface in which the couple due to  $[\text{Fe}(\text{HBpz}_3)_2]$  ceases to increase and the reduction of **1** no longer decreases. In an attempt to show that the steady state represents only diffusion to and from the electrode surface and does not involve a reaction pathway that, after re-oxidation of  $\text{Fe}(\text{HBpz}_3)_2$ , reforms **1**, CV experiments were performed in acetonitrile with  $0.1$  M TBAA as the supporting electrolyte. First,  $[\text{Fe}(\text{HBpz}_3)_2]^+$  was stirred in this electrolyte to determine that no new electroactive species would form during redox cycling in the presence of 100-fold excess acetate ion. Next, **1** was examined in the same electrolyte to see if the presence of excess acetate could inhibit the decomposition of **1** to the mononuclear species during the CV scan. When a single scan CV of **1** from  $0.7$  to  $-1.2$  V was run, however, the results were similar to those found by using TBAP as the supporting electrolyte. The relative peak heights of the reduction wave of **1** to the oxidation wave of  $\text{Fe}(\text{HBpz}_3)_2$  remained the same. Clearly no simple equilibrium exists between the reduced iron containing species after the reduction of **1** involving free acetate that can alter the formation of  $[\text{Fe}(\text{HBpz}_3)_2]$ . The above studies were extended to include the use of platinum and gold electrodes and solvents methylene chloride and dimethylformamide (DMF) with qualitatively similar results. One striking difference between the CV's of **1** in DMF and acetonitrile appeared, however. In DMF at  $200$  mV/s, after the major reduction wave at  $-0.78$  V there is a second (small) reduction at  $-0.92$  V. At slow scan speeds ( $20$  mV/s) this second reduction disappears, but at high scan speeds ( $5$  V/s) the first reduction at  $-0.86$  V is followed by a second reduction at  $-1.04$  V of significant current height. This second wave may represent the reduction of the second iron in a partially reduced, intact form of **1**. It must be noted, however, that under no conditions was an oxidation wave corresponding to either of these reductions found. Thus **1** does not form stable reduced products corresponding to the deoxy or semimet forms of hemerythrin.

(62) Bard, A. J.; Faulkner, L. R. "Electrochemical Methods"; John Wiley & Sons: New York, 1983.

(63) Sharp, P. R.; Bard, A. J. *Inorg. Chem.* **1983**, *19*, 2689-2693.

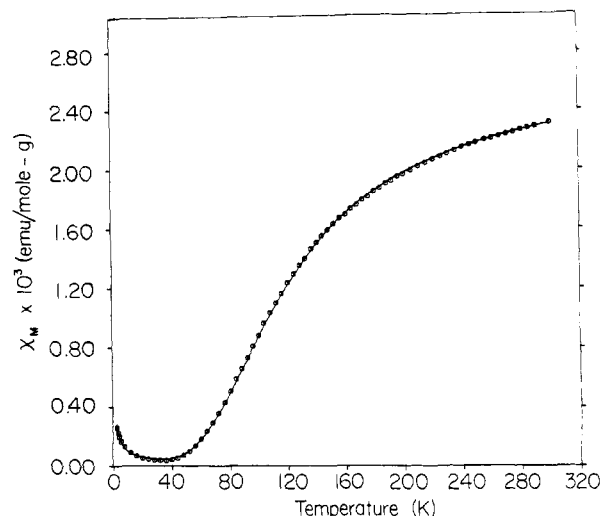


Figure 10. Plot of  $\chi_M^{\text{corr}}$  vs.  $T$  for solid **1**.

**Magnetic Susceptibility.** Measurements were carried out for solution samples of **1** and **2** and for a solid sample of **1**. Room-temperature magnetic moments in  $\text{CDCl}_3$  were measured by using the Evans NMR technique.<sup>27</sup> Molar magnetic susceptibilities were calculated by using eq 3, where  $\Delta\nu$  (Hz) is the shift difference

$$\chi_M = -\frac{3}{4\pi} \frac{\Delta\nu}{\nu} \frac{1000}{c} + M\chi_o - \chi_{\text{dia}} \quad (3)$$

of sample and reference signals,  $\nu$  is the spectrometer frequency,  $c$  is the molar concentration,  $M$  is the molecular weight,  $\chi_o$  is the solvent mass susceptibility, and  $\chi_{\text{dia}}$  is the molar diamagnetic correction for solute. A term involving the density difference between sample and reference solutions was omitted. For **1**,  $\mu_{\text{eff}}/\text{Fe} = 1.71 \mu_B$ , and for **2**  $\mu_{\text{eff}} = 1.72 \mu_B$ .

A plot of molar susceptibility vs. temperature for solid **1**, measured by SQUID susceptometry, is given in Figure 10. This variable temperature behavior of **1** is well described by the theory of Heisenberg, Dirac, and van Vleck for magnetic coupling in a binuclear system with terms added for temperature-independent paramagnetism (TIP) and the contribution to the observed susceptibility from a paramagnetic impurity. The expression<sup>64</sup> for the temperature-dependent susceptibility may be derived from the general isotropic exchange Hamiltonian,  $H = -2J S_1 \cdot S_2$  for  $S_1 = S_2 = 5/2$ , and is given as the first term in eq 4, where  $C =$

$$\chi_M = \frac{2e^{2x} + 10e^{6x} + 28e^{12x} + 60e^{20x} + 110e^{30x}}{1 + 3e^{2x} + 5e^{6x} + 7e^{12x} + 9e^{20x} + 11e^{30x}} + \text{TIP} + p \frac{4.40}{T} \quad (4)$$

$2Ng^2\mu_B^2/kT$ ,  $x = J/kT$ , TIP is the temperature-independent paramagnetism,  $p$  is the mole percentage of a paramagnetic impurity, and  $4.40/T$  is the expression for the susceptibility of an  $S = 5/2$  impurity. A multiplicative term of  $(1-p)$  for the first two terms was omitted owing to the very small value of  $p$  in this experiment. Least-squares fits to eq 4 were carried out under several conditions. In all cases  $g$  was fixed at 2.00. Using the 61 data points in the range 36-300.2 K and refining only  $J$  while fixing both TIP and  $p$  equal to zero gave  $J = -120.17$  (8)  $\text{cm}^{-1}$  with a correlation coefficient (CC) of 0.999968. Using the same data with only  $p = 0$  and refining  $J$  and TIP gives  $J = -121.71$  (14)  $\text{cm}^{-1}$ ,  $\text{TIP} = 3.6$  (3)  $\times 10^{-5}$  cgs  $\text{mol}^{-1}$ , and  $\text{CC} = 0.999933$ . When all of the data (81 points) in the range 2.9-300.2 K were used in the refinement, allowing  $J$  and  $p$  to vary and setting  $\text{TIP} = 0$ , then  $J = -120.42$  (7)  $\text{cm}^{-1}$ ,  $p = 1.99$  (3)  $\times 10^{-4}$ , and  $\text{CC} = 0.999934$ . Finally, with all data and allowing  $J$ , TIP, and  $p$  to vary one obtains  $J = -121.29$  (10)  $\text{cm}^{-1}$ ,  $\text{TIP} = 2.2$  (2)  $\times 10^{-5}$  cgs  $\text{mol}^{-1}$ ,  $p = 1.74$  (3)  $\times 10^{-4}$ , and  $\text{CC} = 0.999945$ . The solid

(64) O'Connor, C. J. *Prog. Inorg. Chem.* **1982**, *29*, 204-283.

line in Figure 10 was calculated by using these last parameters substituted into eq 4.

The value of  $J$  found here indicates a somewhat stronger coupling between iron atoms than is generally the case in simple  $\mu$ -oxo-bridged iron complexes where  $-J$  falls in the range 80–105  $\text{cm}^{-1}$ .<sup>85,39</sup> An exception is the  $[\text{Fe}(\text{protoporphyrin IX})_2\text{O}]$  complex which has a  $J$  value of  $-132 \text{ cm}^{-1}$ .<sup>65</sup> The met (aquo) form of hemerythrin from *Golfingia gouldii* has a  $J$  value of  $-134 \text{ cm}^{-1}$ ,<sup>66</sup> in reasonably good agreement with the model complex **1**. In contrast, oxyhemerythrin from *G. gouldii* has a relatively small  $J$  of  $-77 \text{ cm}^{-1}$ , which may be due to a weakening of the Fe–O–Fe exchange coupling resulting from interaction of the  $\mu$ -oxo atom with a proton of bound hydroperoxide or some protein side chain.<sup>49</sup> In as much as the Fe–O(oxo) bond distances in **1** are not unusually short and  $J$  is not markedly dependent on the Fe–O–Fe angle, the relatively large exchange constant of the protein and model systems may arise from additional contribution of the bridging acetate groups to the exchange coupling pathway.

**Comparison with Hemerythrin, Ribonucleotide Reductase, and Purple Acid Phosphatase Proteins.** The value of compound **1** as a model for the properties of the protein core may be assessed by comparing its properties with those of the hemerythrin derivatives (Table VI).

The structure of the bridged binuclear  $\{\text{Fe}_2\text{O}(\text{O}_2\text{CR})_2\}$  unit is nearly the same in the model and the diiron cores of the metazido forms of the proteins. The greatest structural deviation is the Fe–O–Fe bridging angle,  $123.6 (1)^\circ$  in **1** and  $135^\circ$  and  $132^\circ$  in metazidohemerythrin and metazidomyohemerythrin, respectively. This angle may be influenced by the capping ligand, tri-1-pyrazolylborate vs. protein-supplied histidines. In a recently reported analogue of **1**<sup>18</sup> with the smaller capping TCN ligand, an even smaller Fe–O–Fe angle is obtained. The iron–oxo bridge bond lengths in **1** are equivalent, as expected intuitively of two irons with identical coordination spheres. This result agrees well with the structure of the metazidomyohemerythrin<sup>3</sup> but not with that of metazidohemerythrin.<sup>4</sup> Further refinement of the latter is awaited with interest. Another common feature to both **1** and metazidomyohemerythrin is the lengthening of Fe–N distances trans to the  $\mu$ -oxo bonds.

The magnetic properties of model and protein are similar with coupling constants  $J$  of  $-121$  and  $-134 \text{ cm}^{-1}$ , respectively. The differences in bridging angle have little effect on the coupling constant, as has been observed in other oxo-bridged complexes.<sup>8b</sup>

Qualitatively, the electronic spectra of **1** and the protein look very similar. In comparing the spectra of **1** and metazido or oxyhemerythrin quantitatively, major differences can be seen in the visible region (400–500 nm) where, in **1**, the spectrum of the exogenous ligand-to-metal charge-transfer bands are missing. In this region the spectra of **1** and the met, methoxy, and met-chlorohemerythrin are more similar, although the  ${}^6\text{A}_1 \rightarrow {}^4\text{T}_2({}^4\text{G})$  transition at 695 nm in the spectrum of **1** is shifted to lower wavelengths in these hemerythrin derivatives. The similarity in the electronic spectra below 400 nm underscores the similar electronic structures of metal–pyrazole and metal–imidazole complexes.

The electronic spectrum of **1** also bears a striking resemblance to that of ribonucleotide reductase from *E. coli*.<sup>56,67</sup> The major difference between the two is in the position of the d–d band at 690 nm in **1** vs. 600 nm in ribonucleotide reductase. This difference is not surprising, however, since the corresponding transition in hemerythrin shifts substantially depending on the bound exogenous ligand (Table VI). The previous objection<sup>56</sup> that a triply bridged  $\{\text{Fe}_2\text{O}(\text{O}_2\text{CR})_2\}$  core was unlikely for the diiron center of ribonucleotide reductase based on the rapid rate of  ${}^{18}\text{O}$  incorporation is now untenable since the present study reveals that **1** also incorporates  ${}^{18}\text{O}$  rapidly. In contrast, the electronic

spectrum of purple acid phosphatase is very different from that of **1**, and this protein probably has a different core geometry.<sup>6,7</sup>

Not surprisingly, the major peak in the Raman spectrum of **1**,  $\nu_5$  at  $528 \text{ cm}^{-1}$ , has its counterpart in the spectra of the methemerythrin and oxyhemerythrin.<sup>46b,49,68,69</sup> In the visible region of the electronic spectrum the greatest enhancement of this  $\nu_5$  vibration, both in **1** and in the protein derivatives, occurs around 520 nm. Another peak in the excitation profile is found at 440 nm in the protein and is also implied by our results on **1** (Figure 6). Both in **1** and in the protein, this band is most enhanced when UV light is used. Since “exogenous” ligands cannot bind to **1**, vibrations derived from such ligands, present in some of the protein derivatives, are absent in the spectrum of **1**. Bands between 750 and  $\sim 800 \text{ cm}^{-1}$  have recently been found in the UV enhanced resonance Raman spectra of metazido- and oxyhemerythrin and assigned to the asymmetric vibration of the Fe–O–Fe unit.<sup>49</sup> A band associated with this unit in **1** occurs at  $804 \text{ cm}^{-1}$ , but we have shown it to be a combination band ( $\nu_d + \nu_s$ ). The true position of  $\nu_a$ ,  $751 \text{ cm}^{-1}$  in the IR, is undetectable in the resonance Raman spectra of **1** even using UV excitation. The corresponding bands in the protein may actually be  $\nu_{as}$  for the ( $\mu$ -oxo)diiron(III) unit, but the possibility that these are actually combination bands comparable to the band at  $804 \text{ cm}^{-1}$  in the spectrum of **1** should also be considered.

The Mössbauer spectrum of **1** is, surprisingly, more similar to that of methemerythrin,<sup>70</sup> and is somewhat less similar to that of metazidohemerythrin (Table VI). Although the metazido derivative is structurally closer to **1**, the methemerythrin, recently found to have a vacant coordination site where the ligands bind in the other derivatives,<sup>71</sup> has a quadrupole splitting (1.57 mm/s) almost identical with that of **1** (1.60 mm/s).

The redox behavior of **1** is quite unlike that of hemerythrin. Reduction of **1** leads to a collapse of the bridging structure and formation of  $\text{Fe}(\text{HBpz}_3)_2$ . While the stability of  $[\text{Fe}(\text{HBpz}_3)_2]$  may drive this reaction, reduction of the diiron(III) center increases its intrinsic lability and makes the oxo bridge more susceptible to cleavage. This observation may have relevance to arguments about the structure of deoxyhemerythrin, where EXAFS evidence suggests that the oxo bridge has, indeed, been modified.<sup>16,72</sup>

Finally, as reported elsewhere,<sup>16</sup> the edge and EXAFS regions of the X-ray absorption spectra of **1** and metazidomyohemerythrin are nearly superimposable, further underscoring the similarities in their geometric and electronic structures.

## Conclusions

Accurate models for the metazido forms of hemerythrin and myohemerythrin have been synthesized. Their structures agree well with those of the  $\{\text{Fe}_2\text{O}(\text{O}_2\text{CR})_2\}$  cores in the proteins. Chemical exchange of the  $\mu$ -oxo-bridging ligand is facile, as monitored by  ${}^{18}\text{O}$  labeling studies. Detailed magnetic, optical spectroscopic, FTIR, and resonance Raman spectroscopic studies have defined the electronic and vibrational properties of the triply bridged diiron core. This information is valuable in assigning related results for hemerythrin derivatives and further supports the proposal that ribonucleotide reductase has a similar diiron center. Proton NMR studies suggest that paramagnetically shifted resonances associated with the  $\{\text{Fe}_2\text{O}(\text{O}_2\text{CCH}_2\text{R})_2(\text{his})_3\}$  unit in met forms of hemerythrin should be observable. Electrochemical reduction of  $[\text{Fe}_2\text{O}(\text{O}_2\text{CCH}_3)_2(\text{HBpz}_3)_2]$  results in cleavage to form mononuclear  $[\text{Fe}(\text{HBpz}_3)_2]$  as the only electroactive product. Model compounds of greater relevance to the functional properties

(68) Freier, S. M.; Duff, L. L.; Shriver, D. F.; Klotz, I. M. *Arch. Biochem. Biophys.* **1980**, *205*, 449–463.

(69) Dunn, J. B. R.; Shriver, D. F.; Klotz, I. M. *Biochemistry* **1975**, *12*, 2689–2695.

(70) (a) Okamura, M. Y.; Klotz, I. M.; Johnson, C. E.; Winter, M. R. C.; Williams, R. J. P. *Biochemistry* **1969**, *8*, 1951–1958. (b) Garbett, K.; Johnson, C. E.; Klotz, I. M.; Okamura, M. Y.; Williams, R. J. P. *Arch. Biochem. Biophys.* **1971**, *142*, 574–583.

(71) Stenkamp, R. E.; Sieker, L. C.; Jensen, L. H. *J. Inorg. Biochem.* **1983**, *19*, 247–253.

(72) Elam, W. T.; Stern, F. A.; McCallum, J. D.; Loehr, J. S. *J. Am. Chem. Soc.* **1983**, *105*, 1919–1923.

(65) Moss, T. H.; Lillenthal, H. P.; Moleski, C.; Smythe, G. A.; McDaniel, M. C.; Caughey, W. S. *J. Chem. Soc., Chem. Commun.* **1972**, 263–264.

(66) Dawson, J. W.; Gray, H. B.; Hoening, H. E.; Rossman, G. R.; Schredder, J. M.; Wang, R.-H. *Biochemistry* **1972**, *11*, 461–465.

(67) Atkin, C. L.; Thelander, L.; Reichard, P.; Lang, G. *J. Biol. Chem.* **1973**, *248*, 7464–7472.

**Table VI.** Selected Structural, Magnetic, and Spectroscopic Properties of Binuclear Iron Containing Proteins and Their Models

A. Structural Properties									
	$[\text{Fe}_2\text{O}(\text{O}_2\text{CCH}_3)_2](\text{HBpz}_3)_2a$	$[\text{Fe}_2\text{O}(\text{O}_2\text{CH})_2](\text{HBpz}_3)_2a$	$[\text{Fe}_2\text{O}(\text{O}_2\text{CCH}_3)_2](\text{TCN})_2b$	azidomet- hemerythrin <sup>c</sup>	azidomet- hemerythrin <sup>c</sup>	azidometmyo- hemerythrin <sup>d</sup>			
Fe-O-Fe angle, deg	123.6 (1)	125.5 (2)	118.3 (5)	135	132	132			
Fe-O $\mu$ -oxo dist., Å	1.780 (2), 1.788 (2)	1.777 (3), 1.785 (3)	1.80 (1), 1.77 (1)	1.89, 1.64	1.80, 1.77	1.80, 1.77			
av Fe-N cis to $\mu$ -oxo, Å	2.15	2.14	2.16	2.25	2.05	2.05			
av Fe-N trans to $\mu$ -oxo, Å	2.19	2.18	2.21	2.26	2.16	2.16			
Fe-Fe dist., Å	3.146 (1)	3.168 (1)	3.064 (5)	3.25	3.26	3.26			
av Fe-O $\mu$ -carboxylate, Å	2.043	2.053	2.03 (2)	2.23	2.13	2.13			
B. Mössbauer and Magnetic Results									
	$[\text{Fe}_2\text{O}(\text{O}_2\text{CCH}_3)_2](\text{HBpz}_3)_2a$	azido- methemerythrin <sup>c</sup>	oxyhemerythrin <sup>c</sup>	metheme- rythrin <sup>c</sup>	chloro- methemerythrin <sup>c</sup>	ribonucleotide reductase (R.R.) <sup>f</sup>			
isomer shift, mm s <sup>-1</sup>	0.52	0.50	0.52, 0.48	0.46	0.50	0.53, 0.44			
quadrupole splitting, mm s <sup>-1</sup>	1.60	1.91	1.92, 1.00	1.57	2.04	1.66, 2.45			
<i>J</i> , cm <sup>-1</sup>	-121		-77	-134		-108			
C. Electronic Spectral Data <sup>g</sup>									
assignment	$[\text{Fe}_3\text{O}-$ $(\text{O}_2\text{CCH}_3)_2]$ $(\text{HBpz}_3)_2$ <sup>a</sup>	$[\text{Fe}_3\text{O}-$ $(\text{O}_2\text{CPh})_2]$ $(\text{HBpz}_3)_2$ <sup>a</sup>	$[\text{Fe}_3\text{O}-$ $(\text{O}_2\text{CCH}_3)_2]$ $(\text{TCN})_2$ <sup>b</sup>	hemerythrin derivatives <sup>h</sup>					
	azidomet	oxy	hydroxy	chloro	oxy	R.R.			
LMCT ( $\text{O}^{2-} \rightarrow \text{Fe}$ ) <sup>i</sup>	262 (3375) 339 (4635) 358 sh	342 (5100) 336 (4500)	286 (2500)	326 (3375) 380 sh (2150)	330 (3400) 360 sh (2725)	320 (3400) 362 (2950)			
exogeneous LMCT and/ or unassigned	457 (505) 492 (460)	455 (480) 490 (430)	412 sh 450 (735) 484 sh	446 (1850) br 530 sh <sup>j</sup>	500 (1100) br 490 sh (375) br	480 sh (275) br 500 (400) br			
<sup>6</sup> A <sub>1</sub> → <sup>4</sup> A <sub>1</sub> , <sup>4</sup> F <sub>1</sub> ( <sup>4</sup> G)	528 sh			680 (95)	750 (100)	656 (90)			
<sup>6</sup> A <sub>1</sub> → <sup>4</sup> T <sub>2</sub> ( <sup>4</sup> G) <sup>k</sup>	695 (70)	691 (65)	711 (19) not reported	1010 (5.1) <sup>k</sup>	990 (5.0) <sup>k</sup>	not reported			
<sup>6</sup> A <sub>1</sub> → <sup>4</sup> T <sub>1</sub> ( <sup>4</sup> G) <sup>k</sup>	995 (3.5)					600 (150) not reported			
D. Vibrational Spectral Data <sup>l</sup>									
	$[\text{Fe}_2\text{O}(\text{O}_2\text{CCH}_3)_2]$ $(\text{HBpz}_3)_2$ <sup>a</sup>	$[\text{Fe}_2\text{O}(\text{O}_2\text{CCH}_3)_2]$ $(\text{TCN})_2$ <sup>b</sup>	azido- methemerythrin	oxy- hemerythrin	chloro- hemerythrin	ribonucleotide reductase			
$\nu_s$ Fe-O-Fe symmetric stretch, cm <sup>-1</sup>	528 (511)		507 (491) <sup>m</sup>	486 (475) <sup>j</sup>	509 <sup>m</sup>	496 (481) <sup>n</sup>			
$\nu_{as}$ Fe-O-Fe asymmetric stretch, cm <sup>-1</sup>	751 (721)	730	770 (730) <sup>j</sup>	757 (707) <sup>j</sup>					
$\delta$ Fe-O-Fe deformation, cm <sup>-1</sup>	278 (269)								

<sup>a</sup>This work. Mössbauer parameters for compound **1** are given for the 4.2 K data. <sup>b</sup>Reference 18. <sup>c</sup>Reference 4. <sup>d</sup>Reference 3. <sup>e</sup>Reference 70, 77 K, and ref 66. <sup>f</sup>Reference 67, 77 K. <sup>g</sup> $\lambda$  reported in nm, and numbers in parentheses are extinction coefficients per iron atom. <sup>h</sup>Reference 46c. <sup>i</sup>Reference 49. <sup>j</sup>Apparent from published spectra, ref 49 and 67. <sup>k</sup>Reference 46a and this work. <sup>l</sup>Number in parentheses is the <sup>18</sup>O shifted value. <sup>m</sup>Reference 68. <sup>n</sup>Reference 5c.

of hemerythrin and related proteins will require ligands that stabilize the bridged binuclear structure in the reduced, diiron(II) state and permit coordination of exogenous ligands at a non-bridging coordination site. Studies to produce such compounds are in progress.

**Acknowledgment.** This work was supported by National Institutes of Health (NIH) Research Grant GM 32134 (to S.J.L.) from the National Institute of General Medical Sciences. W.H.A. gratefully acknowledges support under NCI Training Grant CA-09112. The mass spectra required for this work were provided by the Facility supported by NIH Grant RR 00317 (Principal Investigator Professor K. Biemann) from the Biotechnology

Resources Branch, Division of Research Resources. Raman spectra were obtained at the MIT Regional Laser Center which is a National Science Foundation Regional Instrumentation Facility. The Francis Bitter National Magnet Laboratory is supported by the National Science Foundation.

**Registry No.** 1, 86177-70-0; 2, 89908-14-5; 3, 89890-13-1.

**Supplementary Material Available:** Tables S1-S6 reporting observed and calculated structure factor amplitudes and thermal parameters for all atoms and fixed hydrogen atom positional parameters (38 pages). Ordering information is given on any current masthead page.

## Communications to the Editor

### Opening of the P<sub>4</sub> Molecule: Preparation and Crystal Structure of a Cobalt Complex of a $\eta^4$ -Tetraphosphabutadiene Ligand

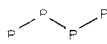
Franco Cecconi, Carlo A. Ghilardi, Stefano Midollini,\* and Annabella Orlandini

*Istituto per lo Studio della Stereochimica ed Energetica dei Composti di Coordinazione C.N.R., 50132 Firenze, Italy*

Received November 21, 1983

Investigations of the reactivity of white phosphorus toward various organometallic compounds have so far provided rather sparse results, most likely because of the well-known "high reactivity" of the P<sub>4</sub> species. Only recently it has been found that P<sub>4</sub> is capable of coordinating to metallic centers as a  $\eta^1$  or  $\eta^2$  ligand.<sup>1,2</sup> More frequently the P<sub>4</sub> molecule has been observed to break apart with subsequent formation of complexes containing the *cyclo*-P<sub>3</sub><sup>3</sup> and -P<sub>2</sub><sup>4</sup> fragments or unsubstituted phosphorus atoms<sup>5</sup> coordinated to the metal.

In this communication we present evidence for the preparation and the crystal structure of a unique complex, [Co-(Ph<sub>2</sub>PCH<sub>2</sub>PPh<sub>2</sub>PPPPPh<sub>2</sub>PCH<sub>2</sub>PPh<sub>2</sub>)]BF<sub>4</sub>, which contains an

unusual zigzag type tetraphosphorus fragment  This complex apparently arises from a P<sub>4</sub> molecule which has been induced to rearrange to a linear P<sub>4</sub> chain by two bis(diphenylphosphino)methane (dppm) ligands.

The preparation of the compound was accomplished by reacting white phosphorus with Co(BF<sub>4</sub>)<sub>2</sub>·6H<sub>2</sub>O and dppm in a THF-1-butanol mixture under N<sub>2</sub>.<sup>6</sup> The complex was a moderately

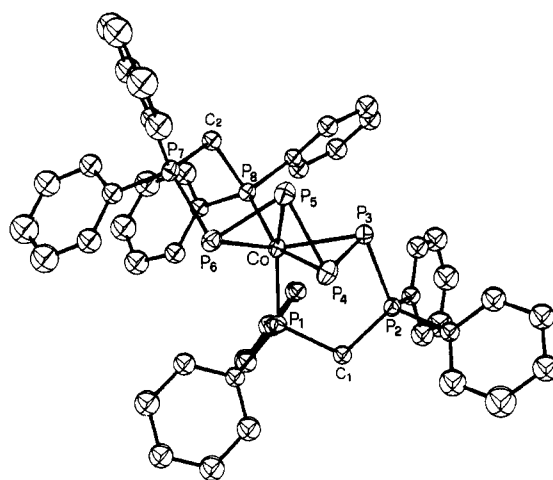


**Figure 1.** Perspective view of the complex cation [Co-(Ph<sub>2</sub>PCH<sub>2</sub>PPh<sub>2</sub>PPPPPh<sub>2</sub>PCH<sub>2</sub>PPh<sub>2</sub>)]<sup>+</sup>. ORTEP drawing with 30% probability ellipsoids.

**Table I.** Selected Bond Distances (Å) and Angles (deg)

Co-P1	2.203 (2)	P2-P3	2.183 (3)
Co-P3	2.281 (2)	P3-P4	2.173 (3)
Co-P4	2.285 (2)	P4-P5	2.197 (3)
Co-P5	2.305 (2)	P5-P6	2.171 (3)
Co-P6	2.281 (2)	P6-P7	2.196 (3)
Co-P8	2.196 (2)		
P1-Co-P3	98.8 (1)	P6-Co-P8	98.1 (1)
P1-Co-P4	95.2 (1)	P2-P3-Co	100.8 (1)
P1-Co-P5	149.9 (1)	P4-P3-Co	61.7 (1)
P1-Co-P6	112.1 (1)	P2-P3-P4	93.4 (1)
P1-Co-P8	109.8 (1)	P3-P4-Co	61.5 (1)
P3-Co-P4	56.8 (1)	P5-P4-Co	61.9 (1)
P3-Co-P5	77.1 (1)	P3-P4-P5	81.6 (1)
P3-Co-P6	130.3 (1)	P4-P5-Co	60.9 (1)
P3-Co-P8	107.1 (1)	P6-P5-Co	61.2 (1)
P4-Co-P5	57.2 (1)	P4-P5-P6	86.2 (1)
P4-Co-P6	81.6 (1)	P5-P6-Co	62.3 (1)
P4-Co-P8	152.7 (1)	P7-P6-Co	100.0 (1)
P5-Co-P6	56.5 (1)	P5-P6-P7	91.8 (1)
P5-Co-P8	99.8 (1)		

air-stable, diamagnetic solid that behaves as an 1:1 electrolyte in methylene chloride solution.

The molecular structure of the title compound has been established by a single-crystal X-ray diffraction study.<sup>7</sup> The solution

(1) Dapporto, P.; Midollini, S.; Sacconi, L. *Angew. Chem., Int. Ed. Engl.* **1979**, *18*, 469.

(2) Lindsell, W. E.; McCullough, K. J.; Welch, A. J. *J. Am. Chem. Soc.* **1983**, *105*, 4487.

(3) Di Vaira, M.; Ghilardi, C. A.; Midollini, S.; Sacconi, L. *J. Am. Chem. Soc.* **1978**, *100*, 2550. Vizi-Orosz, A. *J. Organomet. Chem.* **1976**, *111*, 61.

(4) Campana, C. F.; Vizi-Orosz, A.; Pályi, G.; Markö, L.; Dahl, L. F. *Inorg. Chem.* **1979**, *18*, 3054.

(5) Simon, G. L.; Dahl, L. F. *J. Am. Chem. Soc.* **1973**, *95*, 2175.

(6) A solution of white phosphorus (1.5 mmol) dissolved in THF was added, under a nitrogen atmosphere, to a mixture of Co(BF<sub>4</sub>)<sub>2</sub>·6H<sub>2</sub>O (1 mmol) dissolved in 1-butanol and bis(diphenylphosphino)methane (dppm) (2 mmol) dissolved in THF; the resulting solution was heated to the boiling temperature; the solvents were distilled off until the solution turned deep red and then red crystals of analytical formula C<sub>50</sub>H<sub>44</sub>BCoF<sub>4</sub>P<sub>8</sub> precipitated. The yield amounts to 75% based on Co(BF<sub>4</sub>)<sub>2</sub>·6H<sub>2</sub>O. The complex was recrystallized from methylene chloride/1-butanol.